ACCURATE BAYESIAN META-LEARNING BY ACCURATE TASK POSTERIOR INFERENCE

Anonymous authors
Paper under double-blind review

ABSTRACT

Bayesian meta-learning (BML) enables fitting expressive generative models to small datasets by incorporating inductive priors learned from a set of related tasks. The Neural Process (NP) is a prominent deep neural network-based BML architecture, which has shown remarkable results in recent years. In its standard formulation, NP encodes epistemic uncertainty in an amortized, factorized Gaussian variational (VI) approximation to the BML task posterior (TP), using reparametrized gradients. Prior work studies a range of architectural modifications to boost performance, such as attentive computation paths or improved context aggregation schemes, while the influence of the VI scheme remains under-explored. We aim to bridge this gap by introducing GMM-NP, a novel BML model, which builds on recent work that enables highly accurate, full-covariance Gaussian mixture (GMM) TP approximations by combining VI with natural gradients and trust regions. We show that (i) GMM-NP yields tighter evidence lower bounds, increasing the efficiency of marginal likelihood optimization, leading to (ii) improved epistemic uncertainty estimation and accuracy, (iii) without any complex architectural modifications, resulting in a powerful, yet (iv) conceptually simple BML model. GMM-NP outperforms the state of the art on a range of challenging experiments, which highlights its applicability to settings where data is scarce.

1 INTRODUCTION

Driven by algorithmic advances in the field of deep learning (DL) and the availability of increasingly powerful GPU-assisted hardware, the field of machine learning achieved a plethora of impressive results in recent years (Parmar et al., 2018; Radford et al., 2019; Mnih et al., 2015). These were enabled to a large extent by the availability of huge datasets, which enables training expressive deep neural network (DNN) models. In practice, e.g., in industrial settings, such datasets are unfortunately rarely available, rendering standard DL approaches futile. Nevertheless, it is often the case that similar tasks arise repeatedly, such that the number of context examples on a novel target task is typically relatively small, but the joint *meta-dataset* of examples from all tasks accumulated over time can be massive, s.t. powerful inductive biases can be extracted using *meta-learning* (Hospedales et al., 2022). While these inductive biases allow restricting predictions to only those compatible with the meta-data, there typically remains *epistemic uncertainty* due to task ambiguity, as the context data is often not informative enough to identify the target task exactly. *Bayesian meta-learning* (BML) aims at an accurate quantification of this uncertainty, which is crucial for applications like active learning, Bayesian optimization (Shahriari et al., 2016), model-based reinforcement learning (Chua et al., 2018), robotics (Deisenroth et al., 2011), and in safety-critical scenarios.

A prominent BML approach is the Neural Process (NP) (Garnelo et al., 2018b) which employs a DNN-based conditional latent variable (CLV) model, in which the Bayesian belief about the target task is encoded in a factorized Gaussian task posterior (TP) approximation, and inference is amortized over tasks using set encoders (Zaheer et al., 2017). This architecture can be optimized efficiently using variational inference (VI) with standard, reparametrized gradients (Kingma & Welling, 2014). A range of modifications, such as adding deterministic, attentive, computation paths (Kim et al., 2019), or Bayesian set encoders (Volpp et al., 2021), have been proposed in recent years to improve predictive performance. Interestingly, the VI scheme with an amortized, factorized Gaussian TP, optimized using standard gradients, remains largely unaltered. Yet, it is well known that (i) the factorized Gaussian assumption rarely holds in Bayesian learning (MacKay, 2003; Wilson

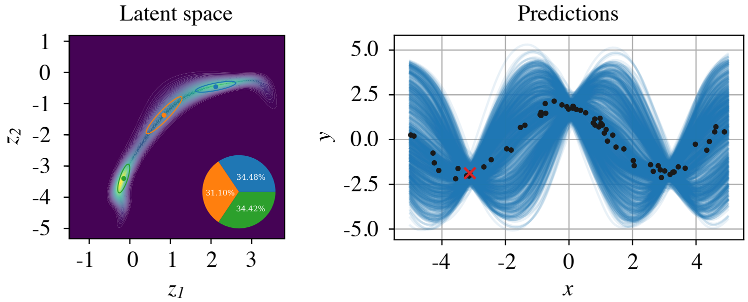

Figure 1: Visualization of our GMM-NP model for a $d_z = 2$ dimensional latent space, trained on a meta-dataset of sinusoidal functions with varying amplitudes and phases, after having observed a single context example (red cross, right panel) from an unseen task (black dots, right panel). Left panel: unnormalized task posterior (TP) distribution (contours) and GMM TP approximation with $K = 3$ components (ellipses, mixture weights in %). Right panel: corresponding function samples from our model (blue lines). A single context example leaves much task ambiguity, reflected in a highly correlated, multi-modal TP. Our GMM approximation correctly captures this: predictions are in accordance with (i) the observed data (all samples pass close to the red context example), and with (ii) the learned inductive biases (all samples are sinusoidal), cf. also Fig. 12 in App. A.5.5

& Izmailov, 2020), (ii) amortized inference can yield suboptimal posterior approximations (Cremer et al., 2018), and (iii) natural gradients are superior to standard gradients for VI in terms of optimization efficiency and robustness (Khan & Nielsen, 2018).

Building on these insights and on recent advances in VI (Lin et al., 2020; Arenz et al., 2022), we propose GMM-NP, a novel NP-based BML algorithm that employs (i) a full-covariance Gaussian mixture (GMM) TP approximation, optimized in a (ii) non-amortized fashion, using (iii) robust and efficient trust region natural gradient (TRNG)-VI. We demonstrate through extensive empirical evaluations and ablations that our approach yields tighter evidence lower bounds, more efficient model optimization, and, thus, markedly improved predictive performance, outperforming the state-of-the-art both in terms of epistemic uncertainty quantification and accuracy. Notably, GMM-NP does not require complex architectural modifications, which shows that accurate TP inference is crucial for accurate BML, an insight we believe will be valuable for future research.

2 Related Work

Multi-task learning aims to leverage inductive biases learned on a meta-dataset of similar tasks for improved data efficiency on unseen target tasks of similar structure. Notable variants include transfer-learning (Zhuang et al., 2020), that refines and combines pre-trained models (Golovin et al., 2017; Krizhevsky et al., 2012), and meta-learning (Schmidhuber, 1987; Thrun & Pratt, 1998; Vilalta & Drissi, 2005; Hospedales et al., 2022), which makes the multi-task setting explicit in the model design by formulating fast adapation mechanisms in order to learn *how* to solve tasks with little context data ("few-shot learning"). A plethora of architectures were studied in the literature, including learner networks that adapt model parameters (Bengio et al., 1991; Schmidhuber, 1992; Ravi & Larochelle, 2017), memory-augmented DNNs (Santoro et al., 2016), early instances of Bayesian meta-models (Edwards & Storkey, 2017; Hewitt et al., 2018), and algorithms that that make use of learned measures of task similarity (Koch et al., 2015; Vinyals et al., 2016; Snell et al., 2017).

Arguably the most prominent meta-learning approaches are the Model-agnostic Meta-learning (MAML) and the Neural Process (NP) model families, due to their generality and flexibility. While the original MAML (Finn et al., 2017) and Conditional NP (Garnelo et al., 2018a) formulations do not explicitly model the epistemic uncertainty arising naturally in few-shot settings due to task ambiguity, both model families were extended to fully Bayesian meta-learning (BML) algorithms that explicitly infer the TP based on a CLV formulation (Heskes, 2000; Bakker & Heskes, 2003). Important representatives are Probabilistic MAML (Grant et al., 2018; Finn et al., 2018) and Bayesian MAML (Kim et al., 2018), as well as several NP-based BML approaches that inspire our work. These include the Standard NP (Garnelo et al., 2018b), which was extended by attentive computation paths to avoid underfitting (Kim et al., 2019), or by Bayesian set encoders (Zaheer et al., 2017; Wagstaff et al., 2019; Volpp et al., 2020) for improved handling of task ambiguity, as well as by hierarchical (Wang & Van Hoof, 2020), bootstrapped (Lee et al., 2020), or graph-based (Louizos et al., 2019) latent distributions. While Monte-Carlo (MC)-based objective functions were considered

(Gordon et al., 2019; Volpp et al., 2021), the traditional NP formulation optimizes a VI objective, inspired by amortized, reparametrized, stochastic gradient VI (Kingma & Welling, 2014; Rezende et al., 2014).

From a more general perspective, VI emerged as a central tool in many areas of probabilistic machine learning, which require tractable approximations of intractable probability distributions, typically arising as the posterior in Bayesian models (Gelman et al., 2004; Koller & Friedman, 2009; Neal, 1996; Wilson & Izmailov, 2020). While early approaches (Attias, 2000) allow analytic updates, more complex algorithms employ stochastic gradients w.r.t. the variational parameters (Ranganath et al., 2014; Kingma & Welling, 2014; Blundell et al., 2015). Such approaches are straightforward to implement and computationally efficient for factorized Gaussian variational distributions, but ignore the information geometry of the loss landscape, leading to suboptimal convergence rates (Khan & Nielsen, 2018). Natural gradient (NG)-VI (Amari, 1998) alleviates this problem and recent work (Hoffman et al., 2013; Winn & Bishop, 2005; Khan & Nielsen, 2018; Khan et al., 2018) successfully applies this idea at scale to complex models, requiring only first-order gradient information (Lin et al., 2019). Further extensions enable NG-VI for structured variational distributions such as mixture models by decomposing the NG update into individual updates per mixture component (Arenz et al., 2018; Lin et al., 2020) which, in combination with trust region (TR) step size control (Abdolmaleki et al., 2015; Arenz et al., 2022), yields robust and efficient VI algorithms for versatile and highly expressive variational distributions such as Gaussian mixture models (GMMs).

3 PRELIMINARIES

We now briefly recap the TRNG-VI algorithm (Lin et al., 2020; Arenz et al., 2022) as well as the NP model (Garnelo et al., 2018b), which form the central building blocks of our GMM-NP model.

3.1 TRUST REGION NATURAL GRADIENT VI WITH GAUSSIAN MIXTURE MODELS

Variational Inference. We consider a probability distribution $p\left(\boldsymbol{z}\right)$ over a random variable $\boldsymbol{z} \in \mathbb{R}^{d_z}$, which is intractable in the sense that we know it only up to some normalization constant Z, i.e., $p\left(\boldsymbol{z}\right) = \tilde{p}\left(\boldsymbol{z}\right) / Z$ with $Z = \int p\left(\boldsymbol{z}\right) \mathrm{d}z$ and tractable $\tilde{p}(\boldsymbol{z})$. We seek to approximate $p\left(\boldsymbol{z}\right)$ by a tractable distribution $q_{\boldsymbol{\phi}}\left(\boldsymbol{z}\right)$, parametrized by $\boldsymbol{\phi}$. Variational inference (VI) frames this task as the minimization w.r.t. $\boldsymbol{\phi}$ of the reverse Kullback-Leiber (KL) divergence (Kullback & Leibler, 1951)

$$\mathrm{KL}\left[q_{\boldsymbol{\phi}} \| p\right] \equiv -\mathbb{E}_{q_{\boldsymbol{\phi}}(\boldsymbol{z})}\left[\log \frac{\tilde{p}\left(\boldsymbol{z}\right)}{q_{\boldsymbol{\phi}}\left(\boldsymbol{z}\right)}\right] + \log Z \equiv -\mathcal{L}\left(\boldsymbol{\phi}\right) + \log Z, \tag{1}$$

where we introduced evidence lower bound (ELBO) $\mathcal{L}\left(\boldsymbol{\phi}\right)$. As Z is independent of $\boldsymbol{\phi}$, minimizing the KL divergence is equivalent to maximizing the ELBO.

Natural Gradients. A standard approach employs stochastic, reparametrized gradients w.r.t. $\boldsymbol{\phi}$ (Kingma & Welling, 2014) for optimization. While this is computationally efficient, it ignores the geometry of the statistical manifold defined by the set of probability distributions $q_{\boldsymbol{\phi}}$, which can lead to suboptimal convergence rates (Khan & Nielsen, 2018). A more efficient solution is to perform updates in the *natural gradient* (NG) direction, i.e., the direction of steepest ascent w.r.t. the Fisher information metric (Amari, 1998). State-of-the-art approaches estimate the NG from first-order gradients of $p\left(\boldsymbol{z}\right)$ by virtue of Stein's lemma (Lin et al., 2019), yielding efficient NG-VI algorithms that scale to complex problems (Khan et al., 2018; Lin et al., 2020; Arenz et al., 2022).

Trust Regions. Selecting appropriate step sizes for updates in $\boldsymbol{\phi}$ can be intricate, which is why Abdolmaleki et al. (2015) propose a (zero-order) algorithm that incorporates a *trust region* constraint of the form $\mathrm{KL}\left[q_{\boldsymbol{\phi}} \| q_{\boldsymbol{\phi}_{\text{old}}}\right] \leq \varepsilon$, which restricts the updates in distribution space and can be enforced with manageable computational overhead (a scalar, convex optimization problem in the Lagrangean parameter for the constraint). As shown by Arenz et al. (2022), such trust regions can easily be combined with gradient information, and allow more aggressive updates in comparison to setting the step size directly, while still ensuring robust convergence.

VI with Gaussian Mixture Models. The quality of the approximation depends on the expressiveness of the distribution family $q_{\boldsymbol{\phi}}$. In settings where p corresponds to the Bayesian posterior of complex latent variable models (MacKay, 2003; Wilson & Izmailov, 2020), simple Gaussian approximations do not yield satisfactory results, as p typically is multimodal. In such cases, Gaussian mixture models (GMMs) are an appealing choice, as they provide cheap sampling, evaluation, and marginalization while allowing expressive approximations (Arenz et al., 2018). However, a naive application of VI is futile because gradients are coupled between GMM components, leading to computationally intractable updates. Fortunately, Arenz et al. (2018) and Lin et al. (2020) show that updating the components and weights individually is possible, while preventing a collapse of the approximation onto a single posterior mode. This leads to two state-of-the-art algorithms for NG-VI with variational GMMs, that differ most notably in the way the step sizes for the updates are controlled: iBayes-GMM (Lin et al., 2020), which directly sets step sizes for the updates, and TRNG-VI (Arenz et al., 2022), which employs trust regions for more efficient and robust convergence.

3.2 Bayesian Meta-Learning with Neural Processes

The Multi-Task Latent Variable Model. We aim to fit a generative model to a meta-dataset $\mathcal{D} = \mathcal{D}_{1:L}$, consisting of regression *tasks* $\mathcal{D}_\ell = \{\boldsymbol{x}_{\ell,1:N}, \boldsymbol{y}_{\ell,1:N}\}$ with inputs $\boldsymbol{x}_{\ell,n} \in \mathbb{R}^{d_x}$ and corresponding evaluations $\boldsymbol{y}_{\ell,n} \in \mathbb{R}^{d_y}$ of unknown functions f_ℓ, i.e., $\boldsymbol{y}_{\ell,n} = f_\ell(\boldsymbol{x}_{\ell,n}) + \boldsymbol{\varepsilon}_n$, where $\boldsymbol{\varepsilon}_n$ denotes (possibly heteroskedastic) noise. Tasks are assumed to share statistical structure as formalized in the multi-task CLV model shown to the right, defining the joint probability distribution

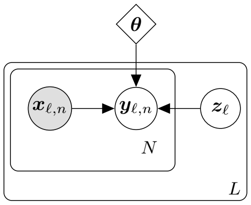

$$p_{\boldsymbol{\theta}}(\boldsymbol{y}_{1:L,1:N}, \boldsymbol{z}_{1:L} | \boldsymbol{x}_{1:L,1:N}) = \prod_{\ell,n} p_{\boldsymbol{\theta}}(\boldsymbol{y}_{\ell,n} | \boldsymbol{x}_{\ell,n}, \boldsymbol{z}_\ell)\, p(\boldsymbol{z}_\ell), \tag{2}$$

where $\boldsymbol{z}_\ell \in \mathbb{R}^{d_z}$ denote latent task descriptors and $\boldsymbol{\theta}$ denotes task-global parameters that capture shared statistical structure. Having observed context data $\mathcal{D}_*^c = \{\boldsymbol{x}_{*,1:M_*}^c, \boldsymbol{y}_{*,1:M_*}^c\} \subset \mathcal{D}_*$ from a target task $\mathcal{D}_*$, predictions are provided in terms of the marginal predictive distribution

$$p_{\boldsymbol{\theta}}(\boldsymbol{y}_{*,1:N_*} | \boldsymbol{x}_{*,1:N_*}, \mathcal{D}_*^c) = \int \prod_n p_{\boldsymbol{\theta}}(\boldsymbol{y}_{*,n} | \boldsymbol{x}_{*,n}, \boldsymbol{z}_*)\, p_{\boldsymbol{\theta}}(\boldsymbol{z}_* | \mathcal{D}_*^c)\, \mathrm{d}z_*, \tag{3}$$

with the *task posterior* (TP) distribution $p_{\boldsymbol{\theta}}(\boldsymbol{z}_* | \mathcal{D}_*^c) = \prod_m p_{\boldsymbol{\theta}}(\boldsymbol{y}_{*,m}^c | \boldsymbol{x}_{*,m}^c, \boldsymbol{z}_*) p(\boldsymbol{z}_*) \,/\, p_{\boldsymbol{\theta}}(\mathcal{D}_*^c)$.

The Neural Process. In its standard formulation, the Neural Process (NP) (Garnelo et al., 2018b) defines a factorized Gaussian likelihood $p_{\boldsymbol{\theta}}(\boldsymbol{y}|\boldsymbol{x}, \boldsymbol{z}) \equiv \mathcal{N}\left(\boldsymbol{y} | \mathrm{dec}_{\boldsymbol{\theta}}^{\boldsymbol{\mu}}(\boldsymbol{x}, \boldsymbol{z}), \mathrm{diag}\left(\sigma_\mathrm{n}^2\right)\right)$, where the *decoder* $\mathrm{dec}_{\boldsymbol{\theta}}^{\boldsymbol{\mu}}$ is a DNN with weights $\boldsymbol{\theta}$, and observation noise variance σ_n^2. As the TP is intractable for this likelihood choice, NP computes a factorized Gaussian approximation $q_{\boldsymbol{\phi}}(\boldsymbol{z}_* | \mathcal{D}_*^c) \equiv \mathcal{N}(\boldsymbol{z}_* | \mathrm{enc}_{\boldsymbol{\phi}}^{\boldsymbol{\mu}}(\mathcal{D}_*^c), \mathrm{diag}(\mathrm{enc}_{\boldsymbol{\phi}}^{\sigma}(\mathcal{D}_*^c)))$ with *deep set encoders* (Zaheer et al., 2017; Wagstaff et al., 2019) $\mathrm{enc}_{\boldsymbol{\phi}}^{\boldsymbol{\mu}}$, $\mathrm{enc}_{\boldsymbol{\phi}}^{\boldsymbol{\sigma}}$, parametrized by $\boldsymbol{\phi}$. The parameters $\boldsymbol{\Phi} \equiv (\boldsymbol{\theta}, \boldsymbol{\phi})$ are optimized jointly on the meta-data by stochastic gradient ascent on the ELBO $\sum_{\ell=1}^L \mathcal{L}_\ell(\boldsymbol{\Phi})$ w.r.t. the approximate log marginal predictive likelihood defined by

$$\log q_{\boldsymbol{\Phi}}(\boldsymbol{y}_{\ell,1:N} | \boldsymbol{x}_{\ell,1:N}, \mathcal{D}_\ell^c) \equiv \log \int \prod_n p_{\boldsymbol{\theta}}(\boldsymbol{y}_{\ell,n} | \boldsymbol{x}_{\ell,n}, \boldsymbol{z}_\ell)\, q_{\boldsymbol{\phi}}(\boldsymbol{z}_\ell | \mathcal{D}_\ell^c)\, \mathrm{d}z_\ell \tag{4}$$

$$\geq \mathbb{E}_{q_{\boldsymbol{\phi}}(\boldsymbol{z}_\ell | \mathcal{D}_\ell)} \left[\sum_n \log p_{\boldsymbol{\theta}}(\boldsymbol{y}_{\ell,n} | \boldsymbol{x}_{\ell,n}, \boldsymbol{z}_\ell) + \log \frac{q_{\boldsymbol{\phi}}(\boldsymbol{z}_\ell | \mathcal{D}_\ell^c)}{q_{\boldsymbol{\phi}}(\boldsymbol{z}_\ell | \mathcal{D}_\ell)} \right] \equiv \mathcal{L}_\ell(\boldsymbol{\Phi}), \tag{5}$$

where $\mathcal{D}_\ell^c \subset \mathcal{D}_\ell$, and stochastic gradients w.r.t. $\boldsymbol{\phi}$ are estimated using the reparametrization trick (Kingma & Welling, 2014). Note that NP *amortizes* inference (the variational parameters $\boldsymbol{\phi}$ are shared across tasks) and that it re-uses $q_{\boldsymbol{\phi}}(\boldsymbol{z}_\ell | \cdot)$ to compute the variational distribution $q_{\boldsymbol{\phi}}(\boldsymbol{z}_\ell | \mathcal{D}_\ell)$, taking advantage of its deep set encoder, which allows to condition it on datasets of arbitrary size.

4 Bayesian Meta-Learning with GMM Task Posteriors

Motivation. Our work is motivated by the observation that the current state-of-the-art approach for training NP-based BML models is suboptimal. Concretely, we identify three interrelated issues with the optimization objective Eq. (5):

(I1) **Expressivity of the Variational Distribution.** $q_{\boldsymbol{\phi}}$ is a (i) factorized, (ii) unimodal Gaussian distribution, (iii) amortized over tasks. In effect, this parametrization only allows crude approximations of the TP distribution (MacKay, 2003; Cremer et al., 2018).

(I2) **Optimization of the Variational Parameters.** (i) Naive gradients of Eq. (5), ignoring the information geometry of $q_{\boldsymbol{\phi}}$, with (ii) direct step size control are employed for optimization, yielding brittle convergence at suboptimal rates (Khan & Nielsen, 2018; Arenz et al., 2022).

(I3) **Optimization of the Model Parameters.** Due to the suboptimal VI scheme (I1,I2), the TP approximation is poor, resulting in a loose ELBO Eq. (5). In effect, optimization w.r.t. the model parameters $\boldsymbol{\theta}$ is inefficient, cf. App. A.1.4 for a detailed discussion.

Armed with these insights, we develop a novel BML model algorithm that is close in spirit to the NP but solves (I1-I3) through TRNG-VI with GMM TP approximations.

Model. Our algorithm builds on the standard multi-task CLV Eq. (2) and retains the likelihood parametrization using a decoder DNN, $\mathrm{dec}_{\boldsymbol{\theta}}^{\boldsymbol{\mu}}(\boldsymbol{x}, \boldsymbol{z})$, as this allows for expressive BML models. Under this parametrization, the log marginal likelihood for a single task reads

$$\log p_{\boldsymbol{\theta}}\left(\boldsymbol{y}_{\ell,1:N} | \boldsymbol{x}_{\ell,1:N}\right) = \log \int \prod_n p_{\boldsymbol{\theta}}\left(\boldsymbol{y}_{\ell,n} | \boldsymbol{x}_{\ell,n}, \boldsymbol{z}_\ell\right) p\left(\boldsymbol{z}_\ell\right) \mathrm{d}z_\ell \equiv \log Z_\ell\left(\boldsymbol{\theta}\right), \tag{6}$$

where $Z_\ell(\boldsymbol{\theta})$ is the normalization constant of the TP $p_{\boldsymbol{\theta}}(\boldsymbol{z}_\ell|\mathcal{D}_\ell) = \tilde{p}_\ell(\boldsymbol{z}_\ell) \,/\, Z_\ell(\boldsymbol{\theta})$ with $\tilde{p}(\boldsymbol{z}_\ell) \equiv \prod_n p_{\boldsymbol{\theta}}(\boldsymbol{y}_{\ell,n}|\boldsymbol{x}_{\ell,n}, \boldsymbol{z}_\ell)\, p(\boldsymbol{z}_\ell)$. In contrast to Eq. (4), we do not condition the left hand side on a context set $\mathcal{D}_\ell^c$, which yields a tractable integrand $\tilde{p}(\boldsymbol{z}_\ell)$ that does not require further approximation. To tackle (I1), we approximate $p_{\boldsymbol{\theta}}(\boldsymbol{z}_\ell|\mathcal{D}_\ell)$ by an expressive variational GMM of the form

$$q_{\boldsymbol{\phi}_\ell}\left(\boldsymbol{z}_\ell\right) \equiv \sum_k w_{\ell,k} q_{\boldsymbol{\phi}_\ell}\left(\boldsymbol{z}_\ell | k\right) \equiv \sum_k w_{\ell,k} \mathcal{N}\left(\boldsymbol{z}_\ell | \boldsymbol{\mu}_{\ell,k}, \boldsymbol{\Sigma}_{\ell,k}\right), \quad \sum_k w_{\ell,k} = 1, \tag{7}$$

where we train individual GMMs with parameters $\boldsymbol{\phi}_\ell \equiv \{w_{\ell,k}, \boldsymbol{\mu}_{\ell,k}, \boldsymbol{\Sigma}_{\ell,k}\}$, $k \in \{1, \ldots, K\}$ for each task ℓ, to not impair approximation quality by introducing inaccuracies through amortization.

Update Equations for the Variational Parameters. To ensure efficient and robust optimization of $\boldsymbol{\phi}_\ell$ (I2), we employ TRNG-VI as proposed by Arenz et al. (2022), with the update equations

$$\boldsymbol{\Sigma}_{\ell,k,\text{new}} = \left[\frac{\eta}{\eta+1}\boldsymbol{\Sigma}_{\ell,k,\text{old}}^{-1} - \frac{1}{\eta+1}\boldsymbol{R}_{\ell,k}\right]^{-1}, \tag{8a}$$

$$\boldsymbol{\mu}_{\ell,k,\text{new}} = \boldsymbol{\Sigma}_{\ell,k,\text{new}}\left[\frac{\eta}{\eta+1}\boldsymbol{\Sigma}_{\ell,k,\text{old}}^{-1}\boldsymbol{\mu}_{\ell,k,\text{old}} + \frac{1}{\eta+1}\left(\boldsymbol{r}_{\ell,k} - \boldsymbol{R}_{\ell,k}\boldsymbol{\mu}_{\ell,k,\text{old}}\right)\right], \tag{8b}$$

$$w_{\ell,k,\text{new}} \propto \exp \rho_{\ell,k}, \tag{8c}$$

where $\boldsymbol{R}_{\ell,k}$, $\boldsymbol{r}_{\ell,k}$, and $\rho_{\ell,k}$ are defined as expectations that can be approximated from per-component samples using MC and require at most first-order gradients of $\tilde{p}(\boldsymbol{z}_\ell)$, which are readily available using standard automatic differentiation software (Abadi et al., 2015; Paszke et al., 2019). Due to space constraints, we move details to App. A.1.1. The optimal value for the trust region parameter $\eta \geq 0$ is defined by a scalar convex optimization problem that can be solved efficiently by a bracketing search, which also ensures positive definiteness of the new covariance matrix $\boldsymbol{\Sigma}_{\ell,k,\text{new}}$.

Updates for the Model Parameters. To optimize the model parameters $\boldsymbol{\theta}$, we decompose the log marginal likelihood $\log Z_\ell(\boldsymbol{\theta})$ according to Eq. (1) as

$$\log Z_\ell\left(\boldsymbol{\theta}\right) = \mathbb{E}_{q_{\boldsymbol{\phi}_\ell}(\boldsymbol{z}_\ell)}\left[\sum_n \log p_{\boldsymbol{\theta}}\left(\boldsymbol{y}_{\ell,n}|\boldsymbol{x}_{\ell,n}, \boldsymbol{z}_\ell\right) + \log\frac{p\left(\boldsymbol{z}_\ell\right)}{q_{\boldsymbol{\phi}_\ell}\left(\boldsymbol{z}_\ell|\mathcal{D}_\ell\right)}\right] + \mathrm{KL}\left[q_{\boldsymbol{\phi}_\ell}\left(\cdot\right) \| \, p_{\boldsymbol{\theta}}\left(\cdot|\mathcal{D}_\ell\right)\right], \tag{9}$$

where the first term on the right hand side is the ELBO w.r.t. $\log Z_\ell(\boldsymbol{\theta})$, which we denote by $\mathcal{L}(\boldsymbol{\theta})$. We expect $\mathcal{L}(\boldsymbol{\theta})$ to be comparably tight, as our inference scheme allows accurate GMM TP approximations $q_{\boldsymbol{\phi}_\ell}$, s.t., the KL term will be small. Consequently, maximization of $Z_\ell(\boldsymbol{\theta})$ w.r.t. $\boldsymbol{\theta}$ can be performed efficiently by maximization of $\mathcal{L}(\boldsymbol{\theta})$ (I3), cf. also App. A.1.4. As is standard, we use the Adam optimizer (Kingma & Ba, 2015) to perform updates in $\boldsymbol{\theta}$, with MC gradient estimates from samples $\boldsymbol{z}_{\ell,s} \sim q_{\boldsymbol{\phi}_\ell}(\boldsymbol{z}_\ell)$: $\nabla_{\boldsymbol{\theta}}\mathcal{L}(\boldsymbol{\theta}) \propto \sum_{s,n} \nabla_{\boldsymbol{\theta}} \log p_{\boldsymbol{\theta}}(\boldsymbol{y}_{\ell,n}|\boldsymbol{x}_{\ell,n}, \boldsymbol{z}_{\ell,s})$.

Meta-Training. The goal of any BML algorithm is to compute accurate predictions with well-calibrated uncertainty estimates according to Eq. (4), based on samples from the approximate TP $q_{\boldsymbol{\phi}_*}(\boldsymbol{z}_*|\mathcal{D}_*^c) \approx p_{\boldsymbol{\theta}}(\boldsymbol{z}|\mathcal{D}_*^c)$, conditioned on a context set $\mathcal{D}_*^c$ from a target task. During a meta-training stage on meta-data $\mathcal{D}_{1:L}$, we aim to encode inductive biases in the model parameters $\boldsymbol{\theta}$,

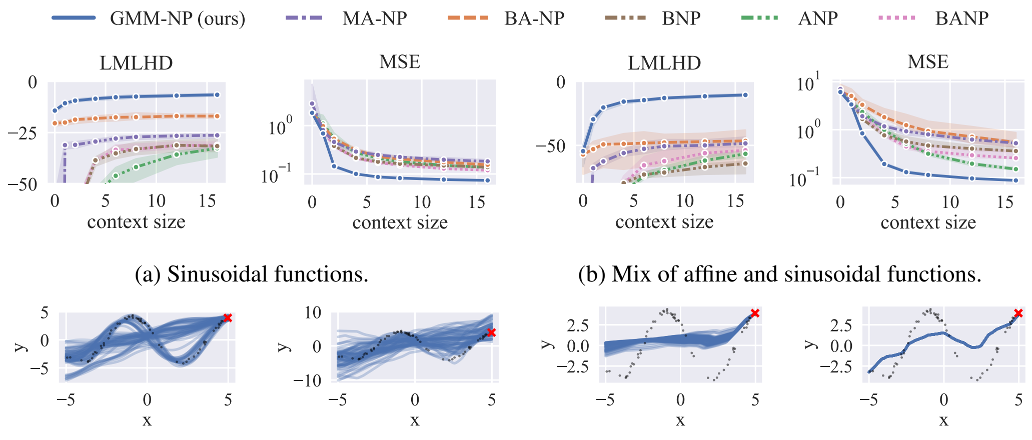

(a) Sinusoidal functions.

(b) Mix of affine and sinusoidal functions.

(c) GMM-NP (ours).

(d) BA-NP.

(e) ANP.

(f) BANP.

Figure 2: Panels (a), (b): LMLHD and MSE on two synthetic function classes. Panels (c) – (f): function samples of models trained on the affine-sinusoidal class (b), given one context example (red) from a sinusoidal instance (black). GMM-NP outperforms the baselines, as it accurately quantifies epistemic uncertainty through diverse samples. BA-NP also shows variability in its samples, but does not achieve competitive performance due to its inaccurate TP approximation. ANP and BANP produce essentially deterministic predictions that fail to give reasonable estimates of the predictive distribution. Cf. also Figs. 10, 11 in App. A.5.4.

s.t. small (few-shot) context sets $\mathcal{D}_*^c$ suffice for accurate predictions. To find versatile solutions that work for variable context set sizes, it is necessary to emulate this during meta-training by evaluating gradients for $\boldsymbol{\theta}$ on samples $\boldsymbol{z}_{\ell,s}$ from approximate TPs informed by a range of context set sizes. Standard NPs achieve this by sampling a minibatch of auxiliary subtasks, with a random number of datapoints, from $\mathcal{D}_{1:L}$ for each step in the parameters $\boldsymbol{\Phi}$ (cf. Sec. A.3.2). Our algorithm uses a similar approach: starting from a fixed set of randomly initialized variational GMMs $\boldsymbol{\phi}_\ell$, and a randomly initialized model $\boldsymbol{\theta}$, we iterate through the meta-data in minibatches of auxiliary subtasks, and perform one update step in $\boldsymbol{\phi}_\ell$ for all subtasks in the minibatch, according to Eqs. (8), followed by one gradient step in $\boldsymbol{\theta}$. Thus, variational and model parameters evolve jointly in a similar fashion as for standard NP, resulting in a meta-training stage with comparable computational complexity, cf. App. A.5.6. As this approach retains a fixed set of variational GMMs over the whole course of meta-training (one for each auxiliary subtask), we accordingly sample a fixed set of auxiliary subtasks at the beginning of meta-training. We summarize our algorithm in App. A.1, Alg. 1.

Predictions. As our architecture does not amortize inference over tasks and, thus, does not learn a set encoder architecture, the variational GMMs learned during meta-training are not required for predictions on test tasks and can be discarded. To make predictions, we fix the model parameters $\boldsymbol{\theta}$ and fit a new variational GMM $q_{\boldsymbol{\phi}_*}$ to $\mathcal{D}_*^c$ by iterating Eqs. (8) until convergence. Afterwards, we can cheaply generate arbitrarily many samples $\boldsymbol{z}_{*,s} \sim q_{\boldsymbol{\phi}_*}(\boldsymbol{z}_*)$, and generate corresponding function samples, evaluated at arbitrary input locations $\boldsymbol{x}_*$, by a single forward pass through the decoder DNN to approximate the predictive distribution according to Eq. (4), cf. App. A.1, Alg. 2.

Discussion of Limitations. As the meta-training stage of GMM-NP requires computational effort comparable to standard NP, the only computational overhead of our algorithm occurs at test time, due to the optimization loop required to fit a variational GMM to $\mathcal{D}_*^c$. While this can be trivially parallelized for multiple test tasks, it incurs a higher computational burden (on the order of 0.1s - 1s per task in our experiments) in comparison to the single forward pass through NP's set encoder, cf. App. A.5.6. We leave a detailed examination for future work, but mention two possible remedies: (i) for problems where test data arrives sequentially, we expect that a few update steps in $\boldsymbol{\phi}_*$ suffice to reach convergence, and (ii) it might be possible to find amortized approximations to Eqs. (8), similar in spirit to standard NP, that retain the advantages of TRNG-VI.

5 Empirical Evaluation

Our empirical evaluation aims to study the effect on the predictive performance of (i) our improved TRNG-VI approach as well as of (ii) expressive variational GMM TP approximations in NP-based BML, in (iii) comparison to the state-of-the-art on (iv) a range of practically relevant meta-learning

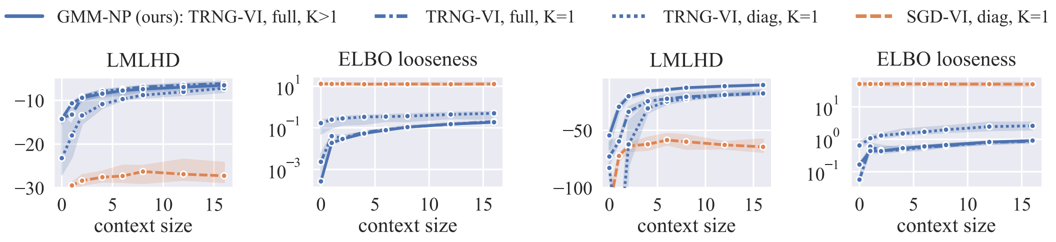

(a) Sinusoidal functions.

(b) Mix of affine and sinusoidal functions.

Figure 3: LMLHD and ELBO looseness over context set size for different versions of our algorithm (blue). Our improved TRNG-VI inference scheme yields tighter ELBOs than standard SGD-VI (orange) and, thus, improved performance (cf. text and App. A.1.4 for details).

tasks. To this end, we evaluate our GMM-NP architecture on a diverse set of BML experiments, and present comparisons to state-of-the-art BML algorithms, namely the original NP with mean context aggregation (MA-NP) (Garnelo et al., 2018b), the NP with Bayesian context aggregation (BA-NP) (Volpp et al., 2021), the Attentive NP (ANP)(Kim et al., 2019), as well as the Bootstrapping (Attentive) NP (B(A)NP) (Lee et al., 2020). Tab. 1 in App. A.2 gives an overview of the architectural differences of these algorithms. We move details on data generation to App. A.4, and on the baseline implementations to App. A.2. For a fair comparison, we employ a fixed experimental protocol for all datasets and models: we first perform a Bayesian hyperparameter search (HPO) to determine optimal algorithm settings, individually for each model-dataset combination. We then retrain the best model with 8 different random seeds and report the median log marginal predictive likelihood (LMLHD) as well as the median mean squared error (MSE), both in dependence of the context set size. To foster reproducibility, we provide further details on our experimental protocol in App. A.3 , the resulting hyperparameters and architecture sizes in App. A.5.7, and publish our source code.[1]

5.1 Synthetic Datasets

We first study two synthetic function classes (Finn et al., 2017; 2018) on which predictions can be easily visualized: (i) sinusoidal functions with varying amplitudes and phases, as well as (ii) a mix of these sinusoidal functions with affine functions with varying slopes and intercepts. Fig. 2 shows that our GMM-NP outperforms all baselines by a large margin over the whole range of context sizes, both in terms of LMLHD and MSE. This indicates that GMM-NP's improved TP approximation indeed yields improved epistemic uncertainty estimation (higher LMLHD). Interestingly, GMM-NP also shows improved accuracy (lower MSE) and, notably, achieves this without any additional architectural modifications like parallel deterministic paths with attention modules. This is particularly pleasing, as the results show that such deterministic paths indeed improve accuracy, but degrade epistemic uncertainty estimation massively: (B)ANP performs worst in terms of LMLHD. This is further substantiated by (i) observing that MA-NP and BA-NP, both of which don't employ deterministic paths, are among the best baselines w.r.t. LMLHD, and (ii) by visualizing model predictions (Figs. 2, 10, 11), demonstrating that (B)ANP compute essentially deterministic function samples that fail to correctly estimate the predictive distribution, while our GMM-NP yields estimates uncertainty well through variable samples. BNP does not achieve competitive performance, presumably because the bootstrapping approach does not work well for small context sets.

5.2 Ablation: Task Posterior Inference

We now demonstrate that GMM-NP's improved performance can indeed be explained by the improved TRNG-VI algorithm with accurate GMM TP approximation. To this end, we compare: (i) BA-NP, i.e., amortized VI with reparameterized gradients and unimodal, factorized Gaussian TP (SGD-VI, diag, $K = 1$), (ii) our GMM-NP, i.e., non-amortized TRNG-VI and full-covariance GMM TP (TRNG-VI, full, $K > 1$), as well as two models employing TRNG-VI, but a unimodal Gaussian TP with (iii) full, and (iv) diagonal covariance. The results are shown in Fig. 3. In addition, we compare (v) an architecture with full-covariance GMM TP, but trained with iBayes-GMM (Lin et al., 2020), i.e., with direct step size control instead of trust regions (Fig. 6, App. A.5.1).

VI Algorithm. Considering the LMLHD metric, we observe a significant performance boost when keeping the traditional factorized Gaussian approximation, but switching from SGD-VI to TRNG-

[1] https://github.com/iclr2023-gmmnp/gmmnp

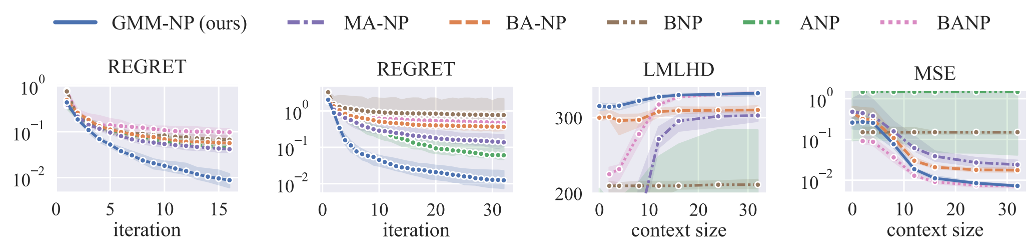

(a) BO on Branin (2D). (b) BO on Hartmann (3D). (c) 4D Furuta dynamics prediction.

Figure 4: Panels (a), (b): simple regret over iteration, when using BML models as Bayesian optimization (BO) surrogates (further results in App. A.5.2). As BO relies on well-calibrated uncertainty predictions, the results demonstrate that GMM-NP provides superior uncertainty estimates. Panel (c): log marginal likelihood (LMLHD) and MSE on one-step ahead predictions of 4D Furuta pendulum dynamics. While GMM-NP generally performs best, BANP also shows strong results.

VI, indicating that the standard SGD-VI approach is indeed suboptimal for BML. To study this further, we estimate the looseness of the ELBO (cf. App. A.3.3), i.e., the median (over tasks) value of the KL divergence $\mathrm{KL}\left[q_{\phi_\ell}\left(\cdot|\mathcal{D}_\ell\right) \| \, p_{\boldsymbol{\theta}}\left(\cdot|\mathcal{D}_\ell\right)\right]$ between the true and approximate TPs. We observe that TRNG-VI provides ELBOs that are tighter by at least one order of magnitude in comparison to SGD-VI. As discussed above, this allows for more efficient optimization of the model parameters $\boldsymbol{\theta}$, explaining the performance gain. Lastly, we find that trust regions yield tighter ELBOs than direct step size control and, consequently, improve predictive performance, cf. Fig. 6, App. A.5.1

Posterior Expressivity. We now study the effect of increasing the expressiveness of the TP approximation. This discussion is supplemented by Fig. 1, where we visualize the TP and its approximation for a $d_z = 2$ dimensional latent space. First, we observe tighter ELBOs and improved performance when considering full-covariance (but still unimodal) Gaussian TP approximations, and this effect is particularly pronounced for small context sets. This is intuitive, as small context sizes leave a lot of task ambiguity, leading to highly correlated latent dimensions (Fig. 1). If we now switch to multimodal TP approximations, i.e., our full GMM-NP architecture with $K > 1$ components (K optimized by HPO), we observe a further increase in performance, as the multimodality of the true TP can be captured more accurately (Figs. 1,12). This effect is especially pronounced for the affine-sinusoidal mix, but also present for the purely sinusoidal function class. As more complex function classes exhibit stronger task ambiguity, the TP will likely exhibit multimodal, correlated structure over wider ranges of context sizes, s.t. an accurate TP approximation will be even more important.

5.3 Bayesian Optimization

One important application area for probabilistic regression models is as the surrogate model of Bayesian optimization (BO), a global black-box optimization algorithm well-known for its sampling efficiency (Shahriari et al., 2016). BO serves as an interesting experiment to benchmark Bayesian models, as it relies on well-calibrated uncertainty estimates in order to trade-off exploration against exploitation, which is crucial for efficient optimization. As proposed by Garnelo et al. (2018b), we use Thompson sampling (Russo et al., 2018) as the BO acquisition function and present results on four function classes: (i) 1D functions sampled from Gaussian process (GP) priors with RBF kernels with varying lengthscales and signal variances (Kim et al., 2019), and (ii) three function classes (Volpp et al., 2020) obtained by randomly translating and scaling the global optimization benchmark functions Forrester (1D) (Forrester et al., 2008), Branin (2D) (Picheny et al., 2013), and Hartmann-3 (3D) (Szego & Dixon, 1978). In Figs. 4a,4b,7, we report the median simple regret, i.e., the difference of the current incumbent value to the function's minimum, over BO iteration. We observe that our GMM-NP model represents a more powerful BO surrogate compared to the baselines, providing further evidence that TRNG-VI with GMM TP approximations yields superior epistemic uncertainty estimates. Due to space constraints, we move the results RBF-GP and 1D Forrester, as well as for the LMLHD and MSE metrics to App. A.5.2, Figs. 7, 8.

5.4 Dynamics Modeling

We further investigate a challenging dynamics modeling problem on a function class obtained by simulating a Furuta pendulum (Furuta et al., 1992), a highly non-linear 4D dynamical system, as proposed by Volpp et al. (2021). The task is to predict the difference of the next system state

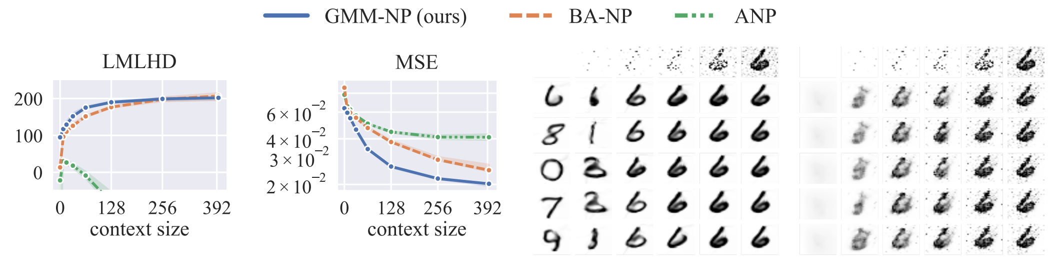

(a) Log marginal likelihood (LMLHD) and MSE. (b) GMM-NP (ours). (c) ANP.

Figure 5: Results on 2D image completion on MNIST. Panels (b),(c) visualize predictions on an unseen task showing the digit "6". The first row shows the context pixels, the remaining rows show five corresponding samples. The results are consistent with earlier observations (e.g., Fig. 2): our GMM-NP model shows highly variable samples for small context sets, yielding an accurate estimate of epistemic uncertainty, and contracts properly around the ground truth when more context information is available. ANP yields crisp predictions but massively overfits to the noise, explaining bad LMLHD and MSE scores. We provide further results in App. A.5.3, Fig. 9.

$\boldsymbol{x}_{\text{next}} \in \mathbb{R}^4$ to the current system state $\boldsymbol{x} \in \mathbb{R}^4$, i.e., we study one-step ahead dynamics predictions $\boldsymbol{x} \to \boldsymbol{y} = \Delta\boldsymbol{x} \equiv \boldsymbol{x}_{\text{next}} - \boldsymbol{x} \in \mathbb{R}^4$. The function class is generated by simulating $L = 64$ episodes of $N = 64$ timesteps each ($\Delta t = 0.1\,\text{s}$), where for each episode we randomly sample the 7 physical parameters of the pendulum (3 lengths, 2 masses, 2 friction coefficients). The results (Fig. 4c) show that GMM-NP outperforms the baselines in terms of LMLHD by a large margin, demonstrating its applicability to complex dynamics prediction tasks where reliable uncertainty estimates are required, e.g., in robotics applications (Deisenroth et al., 2011). Interestingly, while neither ANP nor BNP can reliable solve this task, BANP performs strongly, reaching GMM-NPs asymptotic performance in terms of LMLHD and yielding even slightly better MSE for small context sets.

5.5 Image Completion

To show that our architecture scales to large meta-datasets, we provide results on a 2D image completion experiment on the MNIST database of handwritten digits (LeCun & Cortes, 2010), as proposed by Garnelo et al. (2018b). The task is to predict pixel intensities $\boldsymbol{y} \in \mathbb{R}$ at 2D pixel locations $\boldsymbol{x} \in \mathbb{R}^2$, given a set of context pixels. To obtain a realistic regression task, we add Gaussian noise to each context pixel. The meta-dataset consists of $L = 60000$ images with $N = 784$ pixels each. The results (Fig. 5) are consistent with our previous findings: GMM-NP yields markedly improved performance, outperforming the baselines over the whole range of context sizes. The architectures with deterministic paths ((B)ANP) fail at properly estimating epistemic uncertainties, leading to low LMLHD values, i.p., for large context sizes. Figs. 5b,5c,9 explain why this is the case: GMM-NP (and also, to some extent, BA-NP) generate meaningful images of high variability, corresponding to well-calibrated uncertainty estimates. In contrast, (B)ANP produce essentially deterministic samples that overfit the noise in the context data. While these samples might appear less blurry than those of GMM-NP and BA-NP, they represent inferior solutions of the regression problem.

6 Conclusion and Outlook

We proposed GMM-NP, a novel BML algorithm inspired by the NP model architecture. Our approach focuses on accurate task posterior inference, a central algorithmic building block that until now has been treated by amortized inference with set encoders optimized using standard, reparametrized gradients. We demonstrate that this approach leads to suboptimal task posterior approximations and, thus, inefficient optimization of model parameters. We apply modern TRNG-VI techniques that enable expressive variational GMMs, which yields tight ELBOs, efficient optimization, and markedly improved predictive performance in terms of both epistemic uncertainty estimation and accuracy. Despite its simplicity, GMM-NP outperforms the state-of-the-art on a range of experiments and demonstrates its applicability in practical settings, i.p., when meta and context data is scarce. This demonstrates that complex architectural extensions, like Bayesian set encoders or deterministic, attentive computation paths are not required – in fact, we observe that deterministic modules degrade epistemic uncertainty estimation. Therefore, we hope that our work inspires further research on accurate task posterior inference as this turns out to suffice for accurate BML.

Reproducibility Statement

We took great care to present a fair comparison of our GMM-NP algorithm with the baseline models, with statistically reliable results that can be easily reproduced. In particular, we

- clearly state the hyperparameter settings and hyperparameter optimization procedure we used (Sec. A.3.1),
- clearly state the generating process for the datasets on which we evaluated our algorithm (Sec. A.4),
- concisely define the evaluation metrics we reported (Sec. A.3.3),
- made sure to evaluate these metrics on large test and sample sets, as well as on multiple (8) random seeds, s.t., our results carry statistical significance (Sec. A.3),
- use source code from the original authors for all baselines (Sec. A.2),
- make the source code for our proposed algorithm available online (Sec. A.2).

Ethics Statement

We do not expect any negative ethical or societal impact of our work. I.p., we did not use sensitive/personal data in our experiments.

REFERENCES

Martín Abadi, Ashish Agarwal, Paul Barham, Eugene Brevdo, Zhifeng Chen, Craig Citro, Greg S. Corrado, Andy Davis, Jeffrey Dean, Matthieu Devin, Sanjay Ghemawat, Ian Goodfellow, Andrew Harp, Geoffrey Irving, Michael Isard, Yangqing Jia, Rafal Jozefowicz, Lukasz Kaiser, Manjunath Kudlur, Josh Levenberg, Dandelion Mané, Rajat Monga, Sherry Moore, Derek Murray, Chris Olah, Mike Schuster, Jonathon Shlens, Benoit Steiner, Ilya Sutskever, Kunal Talwar, Paul Tucker, Vincent Vanhoucke, Vijay Vasudevan, Fernanda Viégas, Oriol Vinyals, Pete Warden, Martin Wattenberg, Martin Wicke, Yuan Yu, and Xiaoqiang Zheng. TensorFlow: Large-scale machine learning on heterogeneous systems, 2015. URL `https://www.tensorflow.org/`.

Abbas Abdolmaleki, Rudolf Lioutikov, Jan R Peters, Nuno Lau, Luis Pualo Reis, and Gerhard Neumann. Model-based relative entropy stochastic search. *Advances in Neural Information Processing Systems*, 2015.

Shun-ichi Amari. Natural gradient works efficiently in learning. *Neural Computation*, 1998.

Oleg Arenz, Gerhard Neumann, and Mingjun Zhong. Efficient gradient-free variational inference using policy search. *International Conference on Machine Learning*, 2018.

Oleg Arenz, Philipp Dahlinger, Zihan Ye, Michael Volpp, and Gerhard Neumann. A unified perspective on natural gradient variational inference with Gaussian mixture models. *arXiv*, 2022.

Hagai Attias. A variational Bayesian framework for graphical models. *Advances in Neural Information Processing Systems*, 2000.

Bart Bakker and Tom Heskes. Task clustering and gating for Bayesian multitask learning. *Journal of Machine Learning Research*, 2003.

Yoshua Bengio, Samy Bengio, and Jocelyn Cloutier. Learning a synaptic learning rule. *International Joint Conference on Neural Networks*, 1991.

Lukas Biewald. Experiment tracking with weights and biases, 2020. URL `https://www.wandb.com/`.

Christopher M. Bishop. *Pattern Recognition and Machine Learning*. Springer, 2006.

Charles Blundell, Julien Cornebise, Koray Kavukcuoglu, and Daan Wierstra. Weight uncertainty in neural networks. *International Conference on Machine Learning*, 2015.

Ben Cazzolato and Zebb Prime. On the dynamics of the Furuta pendulum. *Journal of Control Science and Engineering*, 2011.

Kurtland Chua, Roberto Calandra, Rowan McAllister, and Sergey Levine. Deep reinforcement learning in a handful of trials using probabilistic dynamics models. *Advances in Neural Information Processing Systems*, 2018.

Chris Cremer, Xuechen Li, and David Duvenaud. Inference suboptimality in variational autoencoders. *International Conference on Machine Learning*, 2018.

Marc Peter Deisenroth, Gerhard Neumann, and Jan Peters. A survey on policy search for robotics. *Foundations and Trends in Robotics*, 2011.

Harrison A. Edwards and Amos J. Storkey. Towards a neural statistician. *International Conference on Learning Representations*, 2017.

Chelsea Finn, Pieter Abbeel, and Sergey Levine. Model-agnostic meta-learning for fast adaptation of deep networks. *International Conference on Machine Learning*, 2017.

Chelsea Finn, Kelvin Xu, and Sergey Levine. Probabilistic model-agnostic meta-learning. *Advances in Neural Information Processing Systems*, 2018.

Alexander I. J. Forrester, Andras Sobester, and Andy J. Keane. *Engineering Design via Surrogate Modelling - A Practical Guide*. Wiley, 2008.

K. Furuta, M. Yamakita, and S. Kobayashi. Swing-up control of inverted pendulum using pseudo-state feedback. *Journal of Systems and Control Engineering*, 1992.

Marta Garnelo, Dan Rosenbaum, Christopher Maddison, Tiago Ramalho, David Saxton, Murray Shanahan, Yee Whye Teh, Danilo Rezende, and S. M. Ali Eslami. Conditional neural processes. *International Conference on Machine Learning*, 2018a.

Marta Garnelo, Jonathan Schwarz, Dan Rosenbaum, Fabio Viola, Danilo Jimenez Rezende, S. M. Ali Eslami, and Yee Whye Teh. Neural processes. *ICML Workshop on Theoretical Foundations and Applications of Deep Generative Models*, 2018b.

Andrew Gelman, John B. Carlin, Hal S. Stern, and Donald B. Rubin. *Bayesian Data Analysis*. Chapman and Hall/CRC, 2nd ed. edition, 2004.

Daniel Golovin, Benjamin Solnik, Subhodeep Moitra, Greg Kochanski, John Karro, and D. Sculley. Google vizier: a service for black-box optimization. *International Conference on Knowledge Discovery and Data Mining*, 2017.

Jonathan Gordon, John Bronskill, Matthias Bauer, Sebastian Nowozin, and Richard E. Turner. Meta-learning probabilistic inference for prediction. *International Conference on Learning Representations*, 2019.

Erin Grant, Chelsea Finn, Sergey Levine, Trevor Darrell, and Thomas L. Griffiths. Recasting gradient-based meta-learning as hierarchical Bayes. *International Conference on Learning Representations*, 2018.

Tom Heskes. Empirical Bayes for learning to learn. *International Conference on Machine Learning*, 2000.

Luke B. Hewitt, Maxwell I. Nye, Andreea Gane, Tommi S. Jaakkola, and Joshua B. Tenenbaum. The variational homoencoder: learning to infer high capacity generative models from few examples. *Conference on Uncertainty in Artificial Intelligence*, 2018.

Matthew D. Hoffman, David M. Blei, Chong Wang, and John W. Paisley. Stochastic variational inference. *Journal of Machine Learning Research*, 2013.

T. Hospedales, A. Antoniou, P. Micaelli, and A. Storkey. Meta-learning in neural networks: a survey. *IEEE Transactions on Pattern Analysis and Machine Intelligence*, 2022.

Mohammad Emtiyaz Khan and Didrik Nielsen. Fast yet simple natural-gradient descent for variational inference in complex models. *International Symposium on Information Theory and Its Applications (ISITA)*, 2018.

Mohammad Emtiyaz Khan, Didrik Nielsen, Voot Tangkaratt, Wu Lin, Yarin Gal, and Akash Srivastava. Fast and scalable Bayesian deep learning by weight-perturbation in Adam. *International Conference on Machine Learning*, 2018.

Hyunjik Kim, Andriy Mnih, Jonathan Schwarz, Marta Garnelo, Ali Eslami, Dan Rosenbaum, Oriol Vinyals, and Yee Whye Teh. Attentive neural processes. *International Conference on Learning Representations*, 2019.

Taesup Kim, Jaesik Yoon, Ousmane Dia, Sungwoong Kim, Yoshua Bengio, and Sungjin Ahn. Bayesian model-agnostic meta-learning. *Advances in Neural Information Processing Systems*, 2018.

Diederik P. Kingma and Jimmy Ba. Adam: a method for stochastic optimization. *International Conference on Learning Representations*, 2015.

Diederik P. Kingma and Max Welling. Auto-Encoding Variational Bayes. *arXiv:1312.6114 [cs, stat]*, 2013.

Diederik P. Kingma and Max Welling. Auto-encoding variational bayes. *International Conference on Learning Representations*, 2014.

Gregory Koch, Richard Zemel, and Ruslan Salakhutdinov. Siamese neural networks for one-shot image recognition. *International Conference on Machine Learning*, 2015.

D. Koller and N. Friedman. *Probabilistic Graphical Models: Principles and Techniques*. MIT Press, 2009.

Alex Krizhevsky, Ilya Sutskever, and Geoffrey E Hinton. Imagenet classification with deep convolutional neural networks. *Advances in Neural Information Processing Systems*, 2012.

S. Kullback and R. A. Leibler. On information and sufficiency. *The Annals of Mathematical Statistics*, 1951.

Yann LeCun and Corinna Cortes. MNIST handwritten digit database. 2010.

Juho Lee, Yoonho Lee, Jungtaek Kim, Eunho Yang, Sung Ju Hwang, and Yee Whye Teh. Bootstrapping neural processes. *Advances in Neural Information Processing Systems*, 2020.

Wu Lin, Mohammad Emtiyaz Khan, and Mark Schmidt. Stein's lemma for the reparameterization trick with exponential family mixtures. *arXiv*, 2019.

Wu Lin, Mark Schmidt, and Mohammad Khan. Handling the positive-definite constraint in the Bayesian learning rule. *International Conference on Machine Learning*, 2020.

Christos Louizos, Xiahan Shi, Klamer Schutte, and M. Welling. The functional neural process. *Advances in Neural Information Processing Systems*, 2019.

David J. C. MacKay. *Information Theory, Inference, and Learning Algorithms*. Cambridge University Press, 2003.

Volodymyr Mnih, Koray Kavukcuoglu, David Silver, Andrei A. Rusu, Joel Veness, Marc G. Bellemare, Alex Graves, Martin Riedmiller, Andreas K. Fidjeland, Georg Ostrovski, Stig Petersen, Charles Beattie, Amir Sadik, Ioannis Antonoglou, Helen King, Dharshan Kumaran, Daan Wierstra, Shane Legg, and Demis Hassabis. Human-level control through deep reinforcement learning. *Nature*, 2015.

Radford M. Neal. *Bayesian Learning for Neural Networks*. Springer-Verlag, 1996.

Niki Parmar, Ashish Vaswani, Jakob Uszkoreit, Lukasz Kaiser, Noam M. Shazeer, Alexander Ku, and Dustin Tran. Image Transformer. *International Conference on Machine Learning*, 2018.

Adam Paszke, Sam Gross, Francisco Massa, Adam Lerer, James Bradbury, Gregory Chanan, Trevor Killeen, Zeming Lin, Natalia Gimelshein, Luca Antiga, Alban Desmaison, Andreas Kopf, Edward Yang, Zachary DeVito, Martin Raison, Alykhan Tejani, Sasank Chilamkurthy, Benoit Steiner, Lu Fang, Junjie Bai, and Soumith Chintala. Pytorch: An imperative style, high-performance deep learning library. *Advances in Neural Information Processing Systems*, 2019.

Victor Picheny, Tobias Wagner, and David Ginsbourger. A benchmark of kriging-based infill criteria for noisy optimization. *Structural and Multidisciplinary Optimization*, 2013.

Alec Radford, Jeff Wu, Rewon Child, David Luan, Dario Amodei, and Ilya Sutskever. Language Models are Unsupervised Multitask Learners. *arXiv*, 2019.

Rajesh Ranganath, Sean Gerrish, and David Blei. Black box variational inference. *International Conference on Artificial Intelligence and Statistics*, 2014.

Sachin Ravi and Hugo Larochelle. Optimization as a model for few-shot learning. *International Conference on Learning Representations*, 2017.

Danilo Jimenez Rezende, Shakir Mohamed, and Daan Wierstra. Stochastic backpropagation and approximate inference in deep generative models. *International Conference on Machine Learning*, 2014.

Daniel J. Russo, Benjamin Van Roy, Abbas Kazerouni, Ian Osband, and Zheng Wen. A tutorial on Thompson sampling. *Foundations and Trends in Machine Learning*, 2018.

Adam Santoro, Sergey Bartunov, Matthew M. Botvinick, Daan Wierstra, and Timothy P. Lillicrap. Meta-learning with memory-augmented neural networks. *International Conference on Machine Learning*, 2016.

Jürgen Schmidhuber. Evolutionary principles in self-referential learning. on learning how to learn: The meta-meta-meta...-hook. Master's thesis, 1987.

Jürgen Schmidhuber. Learning to control fast-weight memories: an alternative to dynamic recurrent networks. *Neural Computation*, 1992.

Bobak Shahriari, Kevin Swersky, Ziyu Wang, Ryan P. Adams, and Nando de Freitas. Taking the Human Out of the Loop: A Review of Bayesian Optimization. *Proceedings of the IEEE*, 2016.

Jake Snell, Kevin Swersky, and Richard S. Zemel. Prototypical networks for few-shot learning. *Advances in Neural Information Processing Systems*, 2017.

G. P. Szego and L. C. W. Dixon. *Towards global optimisation*. North-Holland Pub. Co., 1978.

Sebastian Thrun and Lorien Pratt. *Learning to Learn*. Kluwer Academic Publishers, 1998.

Ricardo Vilalta and Youssef Drissi. A perspective view and survey of meta-learning. *Artificial Intelligence Review*, 2005.

Oriol Vinyals, Charles Blundell, Timothy Lillicrap, Koray Kavukcuoglu, and Daan Wierstra. Matching networks for one shot learning. *Advances in Neural Information Processing Systems*, 2016.

Michael Volpp, Lukas P. Fröhlich, Kirsten Fischer, Andreas Doerr, Stefan Falkner, Frank Hutter, and Christian Daniel. Meta-learning acquisition functions for transfer learning in bayesian optimization. *International Conference on Learning Representations*, 2020.

Michael Volpp, Fabian Flürenbrock, Lukas Großberger, Christian Daniel, and Gerhard Neumann. Bayesian context aggregation for neural processes. *International Conference on Learning Representations*, 2021.

Edward Wagstaff, Fabian B. Fuchs, Martin Engelcke, Ingmar Posner, and Michael A. Osborne. On the limitations of representing functions on sets. *International Conference on Machine Learning*, 2019.

Qi Wang and Herke Van Hoof. Doubly stochastic variational inference for neural processes with hierarchical latent variables. *International Conference on Machine Learning*, 2020.

Andrew Gordon Wilson and Pavel Izmailov. Bayesian deep learning and a probabilistic perspective of generalization. *Advances in Neural Information Processing Systems*, 2020.

J. Winn and C.M. Bishop. Variational message passing. *Journal of Machine Learning Research*, 2005.

Manzil Zaheer, Satwik Kottur, Siamak Ravanbakhsh, Barnabás Póczos, Ruslan Salakhutdinov, and Alexander J. Smola. Deep sets. *Advances in Neural Information Processing Systems*, 2017.

Fuzhen Zhuang, Zhiyuan Qi, Keyu Duan, Dongbo Xi, Yongchun Zhu, Hengshu Zhu, Hui Xiong, and Qing He. A comprehensive survey on transfer learning. *Proceedings of the IEEE*, 2020.

A Appendix

This appendix provides further details that supplement the main part of our paper.

A.1 Algorithmic Details

In this section we lay out the full set of variational update equations and provide pseudocode for our GMM-NP algorithm.

A.1.1 Variational Update Equations

We provide the full set of equations required to compute the TRNG update for the variational parameters $\boldsymbol{\phi}_\ell \equiv \{w_{\ell,k}, \boldsymbol{\mu}_{\ell,k}, \boldsymbol{\Sigma}_{\ell,k}\}$, $k \in \{1, \ldots, K\}$, parametrizing our GMM TP approximation as

$$q_{\boldsymbol{\phi}_\ell}(\boldsymbol{z}_\ell) \equiv \sum_k w_{\ell,k} q_{\boldsymbol{\phi}_\ell}(\boldsymbol{z}_\ell|k) \equiv \sum_k w_{\ell,k} \mathcal{N}(\boldsymbol{z}_\ell|\boldsymbol{\mu}_{\ell,k}, \boldsymbol{\Sigma}_{\ell,k}), \quad \sum_k w_{\ell,k} = 1. \tag{10}$$

The TRNG-VI update equations, as proposed by Arenz et al. (2022), read

$$\boldsymbol{\Sigma}_{\ell,k,\text{new}} = \left[\frac{\eta}{\eta+1}\boldsymbol{\Sigma}^{-1}_{\ell,k,\text{old}} - \frac{1}{\eta+1}\boldsymbol{R}_{\ell,k}\right]^{-1}, \tag{11a}$$

$$\boldsymbol{\mu}_{\ell,k,\text{new}} = \boldsymbol{\Sigma}_{\ell,k,\text{new}}\left[\frac{\eta}{\eta+1}\boldsymbol{\Sigma}^{-1}_{\ell,k,\text{old}}\boldsymbol{\mu}_{\ell,k,\text{old}} + \frac{1}{\eta+1}\left(\boldsymbol{r}_{\ell,k} - \boldsymbol{R}_{\ell,k}\boldsymbol{\mu}_{\ell,k,\text{old}}\right)\right], \tag{11b}$$

$$w_{\ell,k,\text{new}} \propto \exp \rho_{\ell,k}, \tag{11c}$$

where $\boldsymbol{R}_{\ell,k}$, $\boldsymbol{r}_{\ell,k}$, and $\rho_{\ell,k}$ are defined as expectations that can be approximated from per-component samples using MC:

$$\boldsymbol{R}_{\ell,k} = \mathbb{E}_{q_{\boldsymbol{\phi}_{\ell,\text{old}}}(\boldsymbol{z}_\ell|k)}\left[\boldsymbol{\Sigma}^{-1}_{\ell,k,\text{old}}\left(\boldsymbol{z}_\ell - \boldsymbol{\mu}_{\ell,k,\text{old}}\right)\nabla^T_{\boldsymbol{z}_\ell} h_{\ell,k}(\boldsymbol{z}_\ell)\right], \tag{12a}$$

$$\boldsymbol{r}_{\ell,k} = \mathbb{E}_{q_{\boldsymbol{\phi}_{\ell,\text{old}}}(\boldsymbol{z}_\ell|k)}\left[\nabla_{\boldsymbol{z}_\ell} h_{\ell,k}(\boldsymbol{z}_\ell)\right], \tag{12b}$$

$$\rho_{\ell,k} = \mathbb{E}_{q_{\boldsymbol{\phi}_{\ell,\text{old}}}(\boldsymbol{z}_\ell|k)}\left[h_{\ell,k}(\boldsymbol{z}_\ell) - \log q_{\boldsymbol{\phi}_{\ell,\text{old}}}(\boldsymbol{z}_\ell|k)\right]. \tag{12c}$$

Here, we defined

$$h_{\ell,k}(\boldsymbol{z}_\ell) \equiv \log \tilde{p}_\ell(\boldsymbol{z}_\ell) + \log q_{\boldsymbol{\phi}_{\ell,\text{old}}}(\boldsymbol{z}_\ell|k) - \log q_{\boldsymbol{\phi}_{\ell,\text{old}}}(\boldsymbol{z}_\ell). \tag{13}$$

The optimal value for the Lagrangean parameter $\eta \geq 0$ that enforces the trust region constraint

$$\text{KL}\left[q_{\boldsymbol{\phi}} \| q_{\boldsymbol{\phi}_{\text{old}}}\right] \leq \varepsilon, \tag{14}$$

is defined by a scalar convex optimization problem that can be solved efficiently by a bracketing search, which also ensures positive definiteness of the new covariance matrix $\boldsymbol{\Sigma}_{\ell,k,\text{new}}$.

A.1.2 GMM initialization

We provide details on the initialization of the variational GMMs before meta-training and testing. As we use the same procedure for each task, we drop task indices ℓ to avoid clutter. Given a number K of components for the GMM task posterior (TP) $q_{\boldsymbol{\phi}}(\boldsymbol{z})$ Eq. (7), we use a prior $p(\boldsymbol{z})$ with K components. To initialize the means $\boldsymbol{\mu}_k$, covariances $\boldsymbol{\Sigma}_k$, and mixture weights w_k for $k \in \{1, \ldots, K\}$, we use the same simple heuristic as Arenz et al. (2022):

- Draw the means $\boldsymbol{\mu}_k$ from a d_z-dimensional standard Normal distribution,
- The covariances $\boldsymbol{\Sigma}_k$ are initialized as diagonal matrices (with 1 on the diagonal),
- The weights are initialized uniformly as $w_k = 1/K$.

A.1.3 Algorithm Summary

We provide pseudocode for the meta-training stage of our GMM-NP algorithm in Alg. 1 and for the prediction stage in Alg. 2.

Algorithm 1 GMM-NP (Meta-Training)

```
Require: Meta-data $\mathcal{D}_\ell = \{\boldsymbol{x}_{\ell,1:N}, \boldsymbol{y}_{\ell,1:N}\}$, $\ell \in 1:L$
  Sample variably-sized auxiliary tasks $\tilde{\mathcal{D}}_{\tilde{\ell}} = \left\{\boldsymbol{x}_{\tilde{\ell},1:N_{\tilde{\ell}}}, \boldsymbol{y}_{\tilde{\ell},1:N_{\tilde{\ell}}}\right\}$, $\tilde{\ell} \in 1:\tilde{L}$, cf. Sec. A.3.2
  Initialize variational parameters $\boldsymbol{\phi}_{1:\tilde{L}} = \left\{w_{1:\tilde{L},1:K}, \boldsymbol{\mu}_{1:\tilde{L},1:K}, \boldsymbol{\Sigma}_{1:\tilde{L},1:K}\right\}$
  Initialize model parameters $\boldsymbol{\theta}$
  while not converged do
     for each minibatch of tasks $I \subset \left\{1, \ldots, \tilde{L}\right\}$ do
        Sample $\boldsymbol{z}_{\ell,k,s} \sim q_{\boldsymbol{\phi}_\ell}(\boldsymbol{z}_\ell|k)$ for $\ell \in I$, $k \in 1:K$, $s \in 1:S$
        Evaluate $f_{\ell,k}$ on $\boldsymbol{z}_{\ell,k,s}$ and $\tilde{\mathcal{D}}_\ell$ for $\ell \in I$, $k \in 1:K$, $s \in 1:S$, Eq. (13)
        Update variational parameters $\boldsymbol{\phi}_\ell$ for $\ell \in I$, Eq. (8)
        Sample $\boldsymbol{z}_{\ell,s} \sim q_{\boldsymbol{\phi}_\ell}(\boldsymbol{z}_\ell)$ for $\ell \in I$, $s \in 1:S$
        Estimate gradient of ELBO Eq. (9): $\nabla_{\boldsymbol{\theta}}\mathcal{L}(\boldsymbol{\theta}) \propto \sum_{s,n} \nabla_{\boldsymbol{\theta}} \log p_{\boldsymbol{\theta}}(\boldsymbol{y}_{\ell,n}|\boldsymbol{x}_{\ell,n}, \boldsymbol{z}_{\ell,s})$
        Perform step in $\boldsymbol{\theta}$ using Adam
     end for
  end while
  return Model parameters $\boldsymbol{\theta}$
```

Algorithm 2 GMM-NP (Prediction)

```
Require: Context data $\mathcal{D}_*^c = \left\{\boldsymbol{x}_{*,1:M_*}^c, \boldsymbol{y}_{*,1:M_*}^c\right\}$, model parameters $\boldsymbol{\theta}$, target inputs $\boldsymbol{x}_{*,1:N_*}^t$
  Initialize variational parameters $\boldsymbol{\phi}_* = \{w_{*,1:K}, \boldsymbol{\mu}_{*,1:K}, \boldsymbol{\Sigma}_{*,1:K}\}$
  while not converged do
     Sample $\boldsymbol{z}_{*,k,s} \sim q_{\boldsymbol{\phi}_*}(\boldsymbol{z}_*|k)$ for $k \in 1:K$, $s \in 1:S$
     Evaluate $f_{*,k}$ on $\boldsymbol{z}_{*,k,s}$ and $\mathcal{D}_*^c$ for $k \in 1:K$, $s \in 1:S$, Eq. (13)
     Update variational parameters $\boldsymbol{\phi}_*$, Eq. (8)
  end while
  Sample $\boldsymbol{z}_* \sim q_{\boldsymbol{\phi}_*}(\boldsymbol{z}_*)$
  return Predictions $\boldsymbol{y}_{*,n}^t = \mathrm{dec}_{\boldsymbol{\theta}}\left(\boldsymbol{x}_{*,n}^t, \boldsymbol{z}_*\right)$, $n \in 1:N_*$
```

A.1.4 Discussion of Convergence Properties

Convergence of the ELBO. Our algorithm inherits the convergence guarantee of the variational Bayes algorithm as discussed, e.g., in Bishop (2006). In general, convergence of variational Bayes is independent of the concrete optimization strategy used for $(\boldsymbol{\phi}, \boldsymbol{\theta})$: as long as both the E-step (step in $\boldsymbol{\phi}$) and the M-step (step in $\boldsymbol{\theta}$) increase the ELBO objective (first term in Eq. (9)), the algorithm is guaranteed to converge to a local optimum of the ELBO. While in standard, reparametrized, variational Bayes (as employed by the baseline methods studied in Sec. 5) $(\boldsymbol{\phi}, \boldsymbol{\theta})$ are optimized jointly using, e.g., Adam (Kingma & Ba, 2015), our method alternates between a step in $\boldsymbol{\phi}$ using TRNG-VI (Arenz et al., 2022) and a step in $\boldsymbol{\theta}$ using Adam. Nevertheless, both steps increase the ELBO, so our algorithm will converge.

Convergence of the Marginal Likelihood. As discussed in Sec. 4, our GMM-NP algorithm is designed to improve the convergence behaviour w.r.t. the *marginal likelihood* Eq. (9) in comparison to existing NP-based BML approaches. Recall that the convergence guarantee of the classical expectation-maximization (EM) algorithm w.r.t. the marginal likelihood is lost as soon as the E-step becomes intractable, i.e., as soon as the posterior distribution cannot be computed exactly, and, thus, has to be approximated by a variational distribution, cf., e.g., Bishop (2006). This is the case for most models of reasonable complexity, e.g., for the variational autoencoder (Kingma & Welling, 2013) or the NP model family (Garnelo et al., 2018b). Our GMM-NP model is no exception here, as we build on the NP model for which the TP distribution cannot be computed analytically. Convergence of the marginal likelihood when using the ELBO (first term in Eq. (9)) as a surrogate objective is guaranteed if the ELBO is tight after the E-step, which is the setting of the aforementioned EM algorithm and only the case for a perfect TP approximation, i.e., if $\mathrm{KL}(q_{\boldsymbol{\phi}}(\boldsymbol{z}) || p_{\boldsymbol{\theta}}(\boldsymbol{z}|\mathcal{D}^c)) = 0$, cf. also App. A.3.3. For imperfect approximations, the tightness of the bound is controlled by the variational gap $\mathrm{KL}(q_{\boldsymbol{\phi}}(\boldsymbol{z}) || p_{\boldsymbol{\theta}}(\boldsymbol{z}|\mathcal{D}^c)) > 0$. A better approximate posterior $q_{\boldsymbol{\phi}}(\boldsymbol{z})$ yields a tighter ELBO, which in turn brings us closer to the EM setting, i.e., typically improves convergence. Our GMM-NP algorithm builds exactly on this insight: we use an expressive TP approximation by a full-covariance GMM and a powerful optimizer for $\boldsymbol{\phi}$ (TRNG-VI, (Arenz et al., 2022)) to obtain a tighter ELBO than existing BML approaches in order to achieve optimization of the model parameters in a way that efficiently maximizes the marginal likelihood.

Table 1: Comparison of state-of-the-art approaches for Bayesian meta-learning.

	Posterior Approximation	VI Approach	Amortization Mechanism	Deterministic Path
GMM-NP (ours)	Full-covariance GMM	Trust region natural gradient	none	none
MA-NP (Garnelo et al., 2018b)	Factorized Gaussian	Reparametrized SGD	DNN-encoder + mean aggregation	none
BA-NP (Volpp et al., 2021)	Factorized Gaussian	Reparametrized SGD	DNN-encoder + Bayesian aggregation	none
BNP (Lee et al., 2020)	Non-parametric (bootstrapped)	SGD	DNN-encoder + mean aggregation	none
ANP (Kim et al., 2019)	Factorized Gaussian	Reparametrized SGD	Self attention + DNN-encoder + mean aggregation	Cross attention
BANP (Lee et al., 2020)	Non-parametric (bootstrapped)	SGD	Self attention + DNN-encoder + mean aggregation	Cross attention

A.2 BASELINE ALGORITHMS

Tab. 1 gives an overview of the architectural differences of the BML approaches we compared in our empirical evaluation (Sec. 5). To compute our results, we consistently use code by the original authors. We also provide source code for our proposed GMM-NP algorithm:

- MA-NP, ANP:
  `https://github.com/deepmind/neural-processes`,
- BA-NP:
  `https://github.com/boschresearch/bayesian-context-aggregation`,
- BNP, BANP:
  `https://github.com/juho-lee/bnp`.
- Source code four our GMM-NP algorithm:
  `https://github.com/iclr2023-gmmnp/gmmnp`

A.3 Experimental Protocol

To foster reproducibility, we provide details on our experimental protocol.

A.3.1 Model Hyperparameters

To arrive at a fair comparison of our GMM-NP model with the baseline approaches, we optimize model hyperparameters individually for each model-dataset combination presented in Sec. 5. Concretely, we perform a Bayesian hyperparameter sweep with 256 trials for each model-dataset combination over the parameters detailed below. For the image completion experiment on MNIST, we employ a grid search with fewer trials to keep the computational effort manageable. For hyperparameters not mentioned below, we consistently use standard settings proposed by the original authors. To implement the hyperparameter search, we use the wandb sweep functionality (Biewald, 2020).

Observation Noise Parametrization. As detailed in Sec. 3.2, all compared models (including our GMM-NP) employ a Gaussian likelihood of the form

$$p_{\boldsymbol{\theta}}\left(\boldsymbol{y}|\boldsymbol{x},\boldsymbol{z}\right) \equiv \mathcal{N}\left(\boldsymbol{y}|\mathrm{dec}_{\boldsymbol{\theta}}^{\boldsymbol{\mu}}\left(\boldsymbol{x},\boldsymbol{z}\right), \mathrm{diag}\left(\sigma_{\mathrm{n}}^2\right)\right), \tag{15}$$

where the mean is computed by a decoder DNN $\mathrm{dec}_{\boldsymbol{\theta}}^{\boldsymbol{\mu}}$ receiving the input location $\boldsymbol{x}$ and a latent sample $\boldsymbol{z}$. However, different parametrizations of the observation noise variance σ_{n}^2 are used in the literature. As it is not clear which setting is fairest, we also treat the observation noise parametrization as a hyperparameter. Concretely, for each model-dataset combination, we test the following settings for the observation noise (with individual hyperparameter sweeps) and report the best performing one:

1. $\sigma_{\mathrm{n}}^2 = \sigma_{\mathrm{n,true}}^2$ with $\sigma_{\mathrm{n,true}}^2$ being the true noise variance on the data,
2. $\sigma_{\mathrm{n}}^2 \in \mathbb{R}$ is a single float value, optimized jointly with $\boldsymbol{\theta}$,
3. $\sigma_{\mathrm{n}}^2 = \mathrm{dec}_{\boldsymbol{\theta}}^{\boldsymbol{\sigma}}\left(\boldsymbol{x}\right)$, i.e., observation noise is parametrized by a second decoder network, optimized jointly with $\mathrm{dec}_{\boldsymbol{\theta}}^{\boldsymbol{\mu}}$, but receiving only the input location,
4. $\sigma_{\mathrm{n}}^2 = \mathrm{dec}_{\boldsymbol{\theta}}^{\boldsymbol{\sigma}}\left(\boldsymbol{x},\boldsymbol{z}\right)$, i.e., observation noise is parametrized by a second decoder network, optimized jointly with $\mathrm{dec}_{\boldsymbol{\theta}}^{\boldsymbol{\mu}}$, and also receiving both the input location and the latent sample.

For all compared models, and regardless of the parametrization, we bound the observation noise from below using a softplus transformation s.t. $\sigma_{\mathrm{n}} \geq \sigma_{\mathrm{n,min}} = 0.1$, as proposed by (Garnelo et al., 2018b; Kim et al., 2019; Lee et al., 2020).

DNN Architectures. For all experiments and all baseline models, we use encoder and decoder DNNs with two hidden layers. Likewise, our GMM-NP model uses a decoder DNN with two hidden layers. We optimize the number of hidden units per layer within the bounds $\{8, \dots, 64\}$.

Latent Dimensionalities. For baseline models with parametric latent distributions (all except B(A)NP), we optimize the latent dimension d_z within the bounds $\{1, \dots, 64\}$. As our GMM-NP algorithm employs full covariance matrices, we restrict the bounds for d_z to $\{1, \dots, 8\}$ for a fair comparison.

Number of GMM components. For our GMM-NP algorithm, as well as for iBayes-GMM (Lin et al., 2020) used for the comparison in Sec. A.5.1, we optimize the number of GMM components within the bounds $\{1, \dots, 10\}$.

Learning Rates and Trust Region Bounds. All algorithms use the Adam optimizer with standard settings to update DNN weights. We optimize the corresponding learning rates on a log-uniform scale within the bounds $\left[10^{-5}, 10^{-1}\right]$. We use the same settings to optimize the step size for the GMM updates of the variational parameters of the iBayes-GMM algorithm (Lin et al., 2020) used for the comparison in Sec. A.5.1. As proposed by Arenz et al. (2022), we optimize the Lagrangean parameter η of our GMM-NP algorithm using a bracketing search on the interval $\left[10^{-3}, 10^{-1}\right]$.

A.3.2 Auxiliary Subtask Generation for Meta-Training

We describe the procedure to sample auxiliary subtasks during meta-training in more detail, cf. Sec. 4.

Nomenclature. Recall from Sec. 3.2 that we define a *meta-task* as the set of all available (noisy) evaluations $\mathcal{D}_\ell$, $\ell \in \{1, \dots, L\}$ from an unknown function f_ℓ and that each meta-task contains N examples. Thus, a meta-task $\mathcal{D}_\ell$ is all data a BML algorithm has available to learn about f_ℓ during meta-training. A *subtask* of meta-task $\mathcal{D}_\ell$ is defined as an arbitrary subset of $\mathcal{D}_\ell$.

Auxiliary Subtask Sampling. As described in Sec. 4, standard NP meta-training samples auxiliary subtasks from the metadata for each minibatch step in order to provide the decoder with samples from task posterior approximations informed by a range of context sizes. We use the following standard procedure (Garnelo et al., 2018b; Kim et al., 2019; Lee et al., 2020) to sample auxiliary subtasks to evaluate the optimization objectives of the baseline approaches (e.g., Eq. 5 for standard NP). Given a minibatch $I \subset \{1, \dots, L\}$ of meta-tasks $\mathcal{D}_\ell$, $\ell \in I$, we first sample auxiliary subtasks $\tilde{\mathcal{D}}_\ell$ with a size $\tilde{N}$ drawn uniformly from $\tilde{N} \in \{N_{\text{min}} + 1, \dots, N_{\text{max}}\}$ with $N_{\text{min}} \geq 1$ and $N_{\text{max}} \leq N$. Then, we sample context sets $\tilde{\mathcal{D}}_\ell^c \subset \tilde{\mathcal{D}}_\ell$ of size M, drawn uniformly from $M \in \left\{1, \dots, \tilde{N}\right\}$. $\tilde{\mathcal{D}}_\ell^c$ and $\tilde{\mathcal{D}}_\ell$ are then used in Eq. 5 to compute the ELBO objective for the current minibatch.

As described in Sec. 4, our GMM-NP algorithm uses a similar approach: we employ auxiliary subtasks with sizes $\tilde{N}$ drawn uniformly from $\tilde{N} \in \{N_{\text{min}}, \dots, N_{\text{max}}\}$ to evaluate the updates for the variational GMM parameters and the model parameters. Note that our algorithm does not require to sample context sets during meta training from the auxiliary subtasks. Furthermore, recall that we train one variational GMM for each auxiliary subtask and retain those GMMs over the whole course of meta training, so we fix a set of $\tilde{L}$ auxiliary subtasks at the beginning of meta-training (in contrast to standard NPs, which sample new subtasks for each minibatch).

We use the following settings for N_{min}, N_{max} in our experiments: $N_{\text{min}} = 1$, $N_{\text{max}} = N$, except for MNIST image completion where we use $N_{\text{max}} = N/2$.

Further, we use $\tilde{L} = 32L$, except for MNIST image completion where we use $\tilde{L} = 8$.

A.3.3 Metrics

For each model-dataset combination, we retrain the best hyperparameter setting determined according to Sec. A.3.1 with 8 different random seeds used for model initialization, and report the median value together with $(5\%, 95\%)$ percentiles of the metrics computed according to the formulae provided below. For all experiments (except the MNIST image completion experiment), we evaluate all metrics on $L = 256$ unseen test tasks $\mathcal{D}_{1:L}$ with $\mathcal{D}_\ell = \{\boldsymbol{y}_{\ell,1:N}, \boldsymbol{x}_{\ell,1:N}\}$ and $N = 64$, from which we sample context sets $\mathcal{D}_\ell^c \subset \mathcal{D}_\ell$. For the image completion experiment we use $L = 1024$ and $N = 784$ (the number of pixels per image). We report the results in dependence of the context set size.

Log Marginal Predictive Likelihood (LMLHD). For a given task ℓ the LMLHD is defined by Eq. (4), which we restate here for convenience:

$$\log q_{\boldsymbol{\theta}} \left(\boldsymbol{y}_{\ell,1:N} | \boldsymbol{x}_{\ell,1:N}, \mathcal{D}_\ell^c\right) \equiv \log \int \prod_n p_{\boldsymbol{\theta}} \left(\boldsymbol{y}_{\ell,n} | \boldsymbol{x}_{\ell,n}, \boldsymbol{z}_\ell\right) q\left(\boldsymbol{z}_\ell | \mathcal{D}_\ell^c\right) \mathrm{d}z_\ell. \tag{16}$$

Here, we use the generic notation $q\left(\boldsymbol{z}_\ell | \mathcal{D}_\ell^c\right)$ to denote the task posterior TP approximation, the concrete form of which depends on the BML model under consideration. As the integral is analytically intractable, we resort to an MC approximation. To this end, we sample $S = 1024$ samples

$\boldsymbol{z}_{\ell,s} \sim q\left(\boldsymbol{z}_\ell | \mathcal{D}_\ell^c\right)$ in the test set and compute (Volpp et al., 2021)

$$\log q_{\boldsymbol{\theta}}\left(\boldsymbol{y}_{\ell,1:N} | \boldsymbol{x}_{\ell,1:N}, \mathcal{D}_\ell^c\right) \equiv \log \int \prod_{n=1}^{N} p_{\boldsymbol{\theta}}\left(\boldsymbol{y}_{\ell,n} | \boldsymbol{x}_{\ell,n}, \boldsymbol{z}_\ell\right) q\left(\boldsymbol{z}_\ell | \mathcal{D}_\ell^c\right) \mathrm{d}\boldsymbol{z}_\ell \tag{17}$$

$$\approx \log \frac{1}{S} \sum_{s=1}^{S} \prod_{n=1}^{N} p_{\boldsymbol{\theta}}\left(\boldsymbol{y}_{\ell,n} | \boldsymbol{x}_{\ell,n}, \boldsymbol{z}_{\ell,s}\right) \tag{18}$$

$$= -\log S + \operatorname*{logsumexp}_{s=1}^{S} \sum_{n=1}^{N} \log p_{\boldsymbol{\theta}}\left(\boldsymbol{y}_{\ell,n} | \boldsymbol{x}_{\ell,n}, \boldsymbol{z}_{\ell,s}\right). \tag{19}$$

where logsumexp denotes the numerically stable implementation of the function $\log \sum_n \exp(x_n)$, available in any scientific computing framework. We then compute the median of this expression over all tasks of the test set.

Mean Squared Error (MSE). We report the MSE w.r.t. the mean prediction. That is, for a given task ℓ, we again draw $S = 1024$ samples $\boldsymbol{z}_{\ell,s} \sim q\left(\boldsymbol{z}_\ell | \mathcal{D}_\ell^c\right)$ and compute

$$\mathrm{MSE}\left(\boldsymbol{y}_{\ell,1:N}, \boldsymbol{x}_{\ell,1:N}\right) \equiv \frac{1}{N} \sum_{n=1}^{N} \left(\frac{1}{S} \sum_{s=1}^{S} \mathrm{dec}_{\boldsymbol{\theta}}^{\boldsymbol{\mu}}\left(\boldsymbol{x}_{\ell,n}, \boldsymbol{z}_{\ell,s}\right) - \boldsymbol{y}_{\ell,n} \right)^2. \tag{20}$$

We then compute the median of this expression over all tasks of the test set.

ELBO Looseness. For a given task ℓ, we define the ELBO looseness as the KL-divergence between the approximate and true task posteriors. According to Eq. (4), this decomposes as

$$\mathrm{KL}\left[q\left(\boldsymbol{z}_\ell | \mathcal{D}_\ell\right) \| p_{\boldsymbol{\theta}}\left(\boldsymbol{z}_\ell | \mathcal{D}_\ell\right)\right] = \log q_{\boldsymbol{\theta}}\left(\boldsymbol{y}_{\ell,1:N} | \boldsymbol{x}_{\ell,1:N}, \mathcal{D}_\ell^c\right) \tag{21}$$

$$- \mathbb{E}_{q(\boldsymbol{z}_\ell | \mathcal{D}_\ell)}\left[\sum_{n=1}^{N} \log p_{\boldsymbol{\theta}}\left(\boldsymbol{y}_{\ell,n} | \boldsymbol{x}_{\ell,n}, \boldsymbol{z}_\ell\right) + \log \frac{q\left(\boldsymbol{z}_\ell | \mathcal{D}_\ell^c\right)}{q\left(\boldsymbol{z}_\ell | \mathcal{D}_\ell\right)} \right], \tag{22}$$

with $\log q_{\boldsymbol{\theta}}\left(\boldsymbol{y}_{\ell,1:N} | \boldsymbol{x}_{\ell,1:N}, \mathcal{D}_\ell^c\right)$ defined by Eq. (16). The second term is the ELBO,

$$\mathcal{L}\left(\boldsymbol{\theta}, \mathcal{D}_\ell^c, \mathcal{D}_\ell\right) \equiv \mathbb{E}_{q(\boldsymbol{z}_\ell | \mathcal{D}_\ell)}\left[\sum_{n=1}^{N} \log p_{\boldsymbol{\theta}}\left(\boldsymbol{y}_{\ell,n} | \boldsymbol{x}_{\ell,n}, \boldsymbol{z}_\ell\right) + \log \frac{q\left(\boldsymbol{z}_\ell | \mathcal{D}_\ell^c\right)}{q\left(\boldsymbol{z}_\ell | \mathcal{D}_\ell\right)} \right], \tag{23}$$

where we made its dependence on both the test set $\mathcal{D}_\ell$ and the context set $\mathcal{D}_\ell^c \subset \mathcal{D}_\ell$ explicit (in contrast to our notation in the main part of this paper). We say the ELBO is tight if its looseness is zero. Then, $\log q_{\boldsymbol{\theta}}\left(\boldsymbol{y}_{\ell,1:N} | \boldsymbol{x}_{\ell,1:N}, \mathcal{D}_\ell^c\right) = \mathcal{L}\left(\boldsymbol{\theta}, \mathcal{D}_\ell^c, \mathcal{D}_\ell\right)$, and optimization of the ELBO w.r.t. $\boldsymbol{\theta}$ is equivalent to optimization of the LMLHD.

For our ablation study (Sec. 5.2), we estimate the looseness of the ELBO by computing the difference of an importance-weighted MC estimate with proposal distribution $q\left(\boldsymbol{z}_\ell | \mathcal{D}_\ell\right)$ of the LMLHD and an MC estimate of the ELBO Eq. (23) with $S = 1024$ samples $\boldsymbol{z}_{\ell,s} \sim q\left(\boldsymbol{z}_\ell | \mathcal{D}_\ell\right)$. Note that the ELBO looseness does not depend on the context set $\mathcal{D}_\ell^c$ and that slight variations with the context set size reported in Sec. 5.2 arise solely due to approximation inaccuracies.

A.4 Data Generation

We provide details on the meta-datasets we use to train the models we compare in Sec. 5. Concretely, we provide

- the dimension d_x of inputs $\boldsymbol{x}_{\ell,n} \in \mathbb{R}^{d_x}$,
- the domain $\mathcal{C} \subset \mathbb{R}^{d_x}$ from which we uniformly sample $\boldsymbol{x}_{\ell,n}$,
- the dimension d_y of targets $\boldsymbol{y}_{\ell,n} \in \mathbb{R}^{d_y}$,
- an expression for the function $f_\ell : \mathbb{R}^{d_x} \to \mathbb{R}^{d_y}$, s.t., $\boldsymbol{y}_{\ell,n} = f_\ell\left(\boldsymbol{x}_{\ell,n}\right) + \boldsymbol{\varepsilon}$,
- the noise standard deviation σ, s.t., $\varepsilon \sim \mathcal{N}\left(\mathbf{0}, \sigma^2\right)$,
- the number L of meta-tasks and the number N of datapoints for each meta-task.

We denote the uniform distribution on $(a, b)^d \subset \mathbb{R}^d$ by $\mathrm{U}\left(a, b\right)^d$.

Sinusoidal Functions.

- $d_x = 1$,
- $\mathcal{C} = [-5.0, 5.0]$
- $d_y = 1$,
- $f_\ell\left(x\right) = A_\ell \sin\left(x - \phi_\ell\right)$, $A_\ell \sim \mathrm{U}\left(0.1, 5.0\right)$, $\phi_\ell \sim \mathrm{U}\left(0.0, \pi\right)$,
- $\sigma = 0.25$,
- $L = 64$, $N = 16$.

Mix of Affine and Sinusoidal Functions.

- $d_x = 1$,
- $\mathcal{C} = [-5.0, 5.0]$
- $d_y = 1$,
- $f_\ell^1\left(x\right) = a_\ell x + b_\ell$, $a_\ell \sim \mathrm{U}\left(-3.0, 3.0\right)$, $b_\ell \sim \mathrm{U}\left(-3.0, 3.0\right)$,
  $f_\ell^2\left(x\right) = A_\ell \sin\left(x - \phi_\ell\right)$, $A_\ell \sim \mathrm{U}\left(0.1, 5.0\right)$, $\phi_\ell \sim \mathrm{U}\left(0.0, \pi\right)$
  f_ℓ is given either by f_ℓ^1 or f_ℓ^2 with probability 0.5,
- $\sigma = 0.25$,
- $L = 64$, $N = 16$.

RBF-GP samples.

- $d_x = 1$,
- $\mathcal{C} = [-2.0, 2.0]$
- $d_y = 1$,
- f_ℓ is drawn from a Gaussian process prior with RBF kernel with lengthscale $l_\ell \sim \mathrm{U}\left(0.5, 1.0\right)$ and signal variance $s_\ell \sim \mathrm{U}\left(0.5, 1.0\right)$
- $\sigma = 0.1$,
- $L = 64$, $N = 16$.

Forrester 1D.

- $d_x = 1$,
- $d_y = 1$,
- We use the definition of Forrester et al. (2008),
- $\sigma = 0.25$,
- $L = 64$, $N = 16$.

Branin 2D.

- $d_x = 2$,
- $d_y = 1$,
- We use the definition given on `https://www.sfu.ca/~ssurjano/branin.html` and apply translations $\boldsymbol{\tau}_\ell \sim \mathrm{U}\left(-0.25, 0.25\right)^2$ to $\boldsymbol{x}$, and scale the function values by $s_\ell \sim \mathrm{U}\left(0.75, 1.25\right)$
- $\sigma = 0.25$,
- $L = 64$, $N = 16$.

Hartmann 3D.

- $d_x = 3$,
- $d_y = 1$,
- We use the definition given on `https://www.sfu.ca/~ssurjano/hart3.html` and apply translations $\boldsymbol{\tau}_\ell \sim \mathrm{U}\left(-0.25, 0.25\right)^3$ to $\boldsymbol{x}$, and scale the function values by $s_\ell \sim \mathrm{U}\left(0.75, 1.25\right)$
- $\sigma = 0.1$,
- $L = 64$, $N = 16$.

4D Furuta Dynamics Prediction.

- $d_x = 4$,
- $d_y = 4$,
- We use the dynamics equations given in Cazzolato & Prime (2011) to simulate episodes, starting from the pendulum balancing in the upright position. For more details, cf. the explanations in Sec. 5.4.
- Noise is generated by random actions on the joints.
- $L = 64$, $N = 64$.

2D MNIST Image Completion.

- $d_x = 2$,
- $d_y = 1$,
- We use the MNIST handwritten image database (LeCun & Cortes, 2010). Each image corresponds to one task. The input $\boldsymbol{x}$ is the pixel location, the target y is the pixel intensity.
- $\sigma = 0.25$,
- $L = 60000$, $N = 784$.

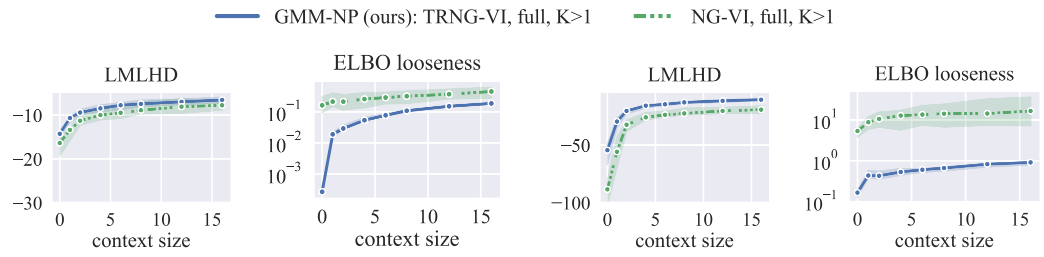

(a) Sinusoidal functions.

(b) Mix of affine and sinusoidal functions.

Figure 6: Log marginal predictive likelihood (LMLHD) and ELBO looseness over context size for our trust region natural gradient VI (TRNG-VI)-based (Arenz et al., 2022) GMM-NP algorithm in comparison to iBayes-GMM (Lin et al., 2020) that uses direct step size control instead of trust regions (NG-VI). Trust regions improve variational optimization, leading to tighter ELBOs, and, consequently, to improved predictive performance.

A.5 Further Experimental Results

We provide further experimental results for the experiments presented in Sec. 5.

A.5.1 Ablation: Trust Regions

In Fig. 6 we compare two methods for step size control for natural gradient VI, namely direct step size control as proposed by (Lin et al., 2020) and trust region step size control (Arenz et al., 2022), as used by our GMM-NP algorithm. We observe that trust regions lead to more robust optimization of the variational parameters, and, thus, to tighter ELBOs. This allows more efficient optimization of the model parameters, leading to improved predictive performance.

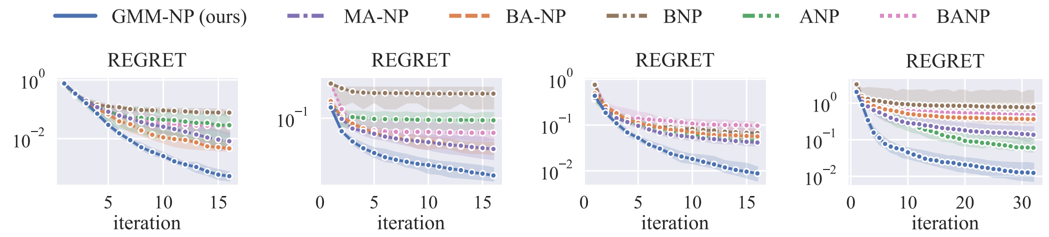

(a) 1D RBF-GP samples. (b) 1D Forrester. (c) 2D Branin. (d) 3D Hartmann.

Figure 7: Simple regret over optimization iteration, when using BML models as Bayesian Optimization (BO) surrogates on various function classes. As BO relies on well-calibrated uncertainty predictions, the results demonstrate that GMM-NP provides superior uncertainty estimates.

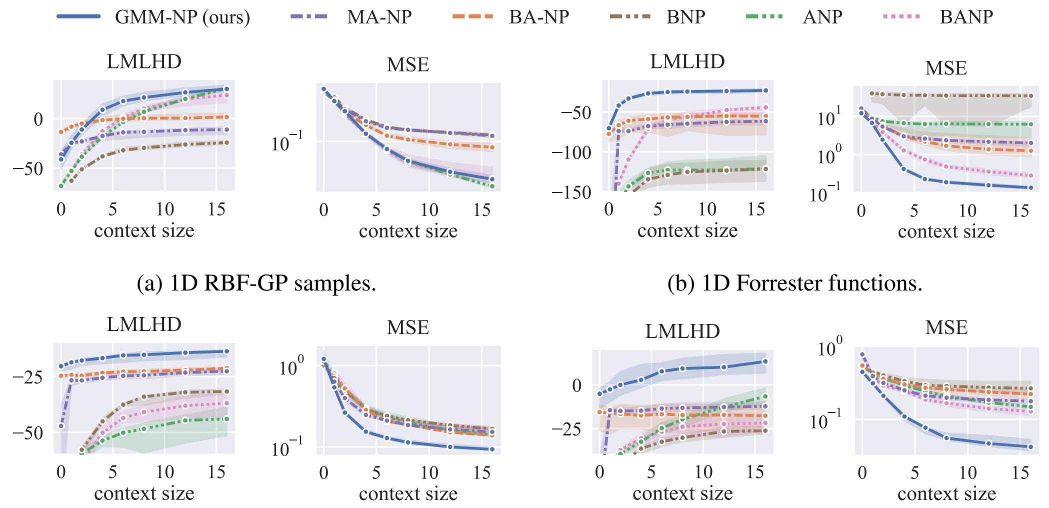

(a) 1D RBF-GP samples. (b) 1D Forrester functions.

(c) 2D Branin functions. (d) 3D Hartmann-3 functions.

Figure 8: Log marginal predictive likelihood (LMLHD) and mean squared error (MSE) over context size for four function classes used to benchmark global optimization algorithms like Bayesian optimization (BO). GMM-NP generally performs favorably, showing accurate predictions with well-calibrated uncertainties.

A.5.2 Bayesian Optimization Experiments

We provide the full set of results for our Bayesian optimzation experiments, cf. Sec. 5.3: Fig. 7 shows the optimization regret for all four evaluated function classes, and Fig. 8 the corresponding results for LMLHD and MSE.

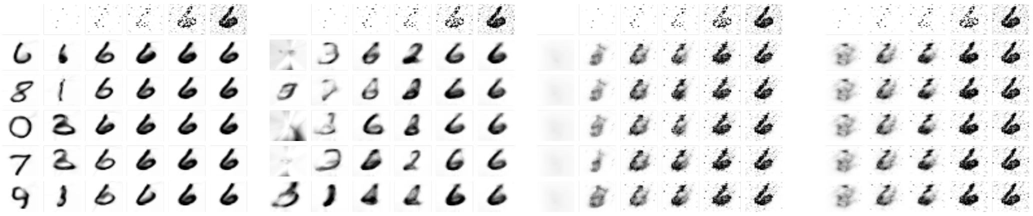
(a) GMM-NP (ours). (b) BA-NP. (c) ANP. (d) BANP.

Figure 9: Predictions on an unseen instance of the MNIST 2D image completion task, showing the digit “6”. The first row of each panel shows the context pixels (ranging from zero pixels in the left column to the full image in the right column). The remaining rows show five samples from the BML models, conditioned on the context pixels shown in the first row. The results are consistent with observations from the other experiments (e.g., Fig. 10): our GMM-NP model shows highly variable samples for small context sets, yielding an accurate estimate of epistemic uncertainty, and contracts properly around the ground truth when more context information is available. BA-NP also shows variable samples, albeit of lower quality. ANP and BANP yield crisp predictions but massively overfit to the noise, explaining their low LMLHD scores. Note also that BANP does not allow predictions for empty context sets.

A.5.3 2D Image Completion on MNIST

Fig. 9 shows the full set of predictions on the 2D image completion experiment on MNIST.

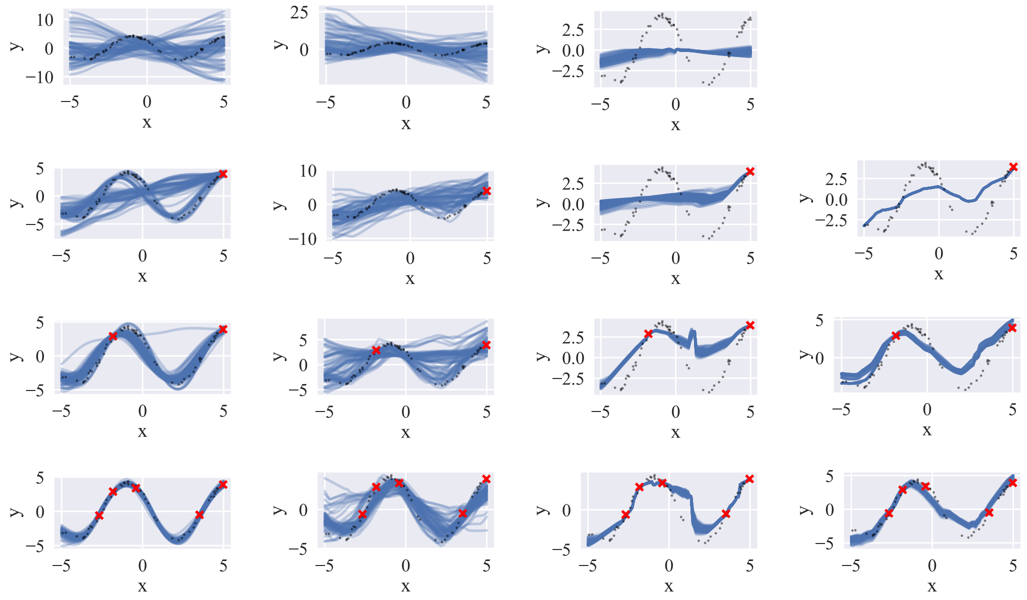

(a) GMM-NP (ours).

(b) BA-NP.

(c) ANP.

(d) BANP.

Figure 10: Function samples computed by various BML models (columns), trained on a function class consisting of a mix of affine and sinusoidal functions (cf. Sec. 5.1), when provided with increasing amounts of context examples (red crosses, rows) from an unseen sinusoidal representative function. We observe that our GMM-NP model accurately quantifies epistemic uncertainty through the variability of its function samples. BA-NP also shows variable samples, but does not achieve the same predictive performance due to its inaccurate approximation of the task posterior distribution. ANP and BANP, both of which employ deterministic computation paths with attention modules, produce essentially deterministic predictions that massively overfit the context data and fail to give a reasonable estimate of the predictive distribution. Therefore, these models have to quantify epistemic uncertainty through the likelihood noise variance, which is ineffective, cf. Fig. 11. Note also that BANP does not provide predictions for empty context sets.

A.5.4 Visualization of Model Predictions

Figs. 10 and Figs. 11 show further visualization of predictions of models trained on the mix of affine and sinusoidal functions.

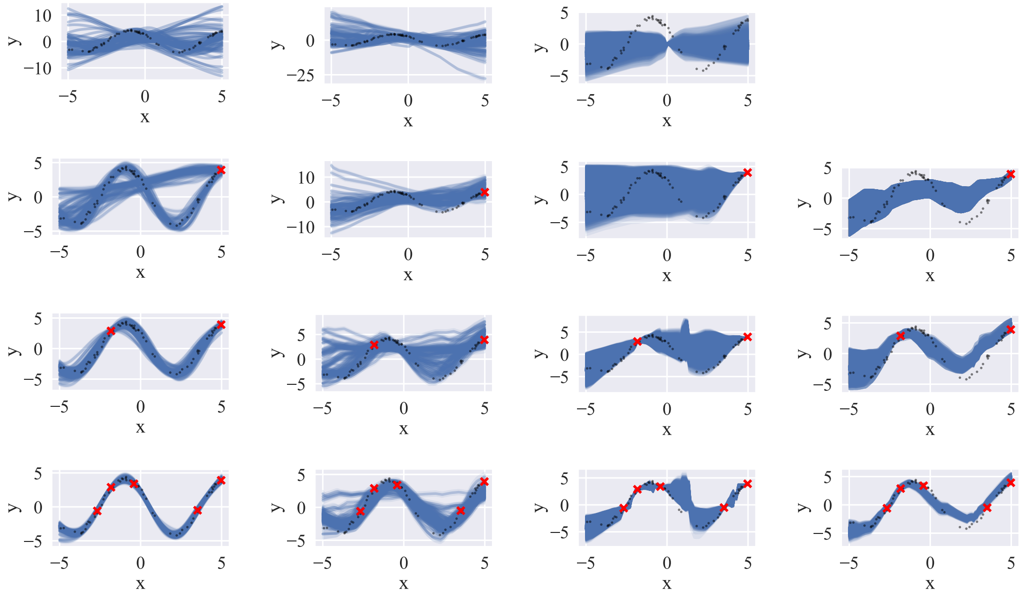

(a) GMM-NP (ours). (b) BA-NP. (c) ANP. (d) BANP.

Figure 11: This figure shows the same data as Fig. 10, but for each function sample we also show a band of ±1 standard deviation of the observation noise, as computed by the decoder DNN. GMM-NP quantifies epistemic uncertainty correctly through its task posterior approximation, and thus does not have to rely on the decoder DNN to quantify epistemic uncertainty through the observation noise. In contrast, ANP and BANP fail to produce variable function samples, and have to make up for that by quantifying epistemic uncertainty through the observation noise, which is ineffective. Note also that BANP does not provide predictions for empty context sets.

A.5.5 Visualization of Latent Space Structure

We provide further visualizations similar to Fig. 1 of the task posterior approximation and corresponding function samples of our GMM-NP, when trained on the sinusoidal function class.

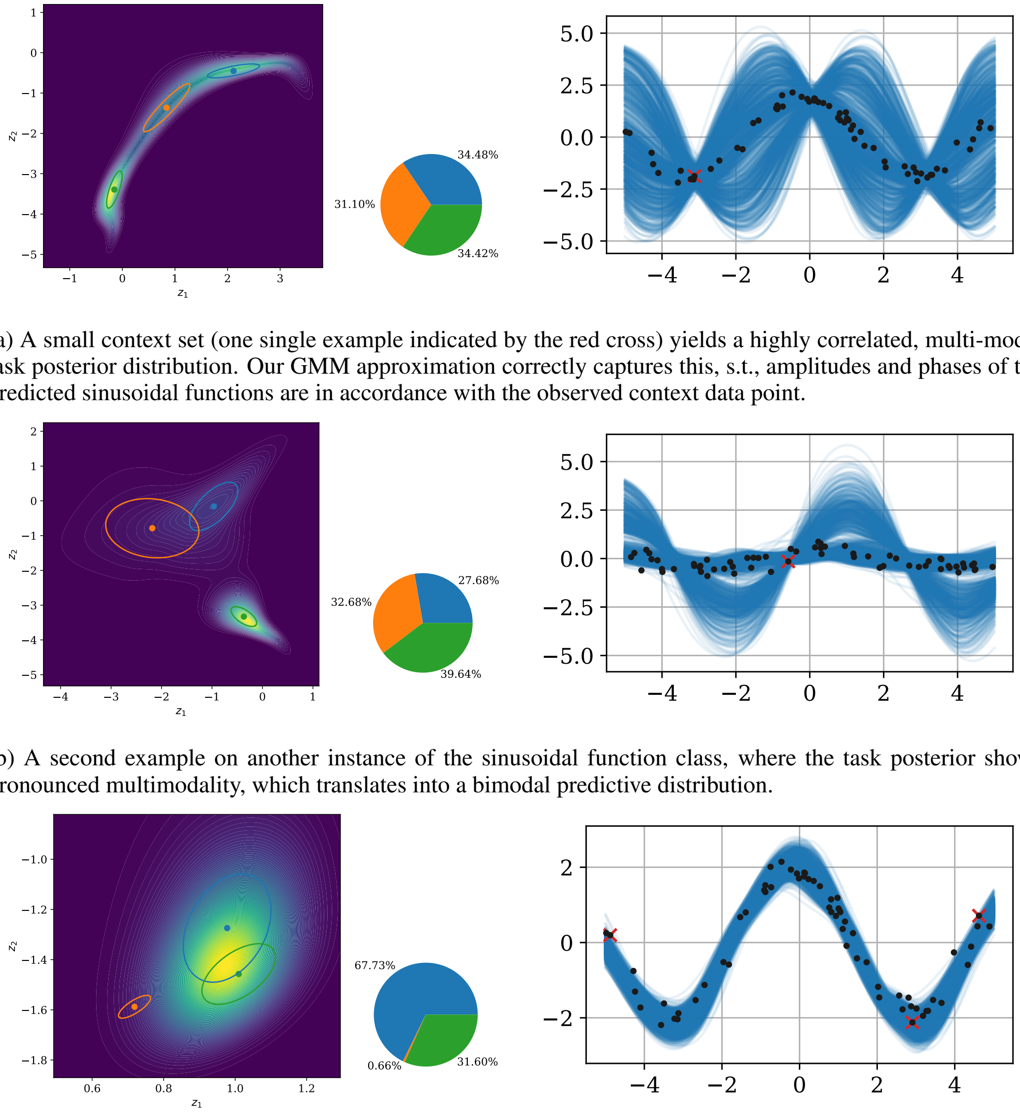

(a) A small context set (one single example indicated by the red cross) yields a highly correlated, multi-modal task posterior distribution. Our GMM approximation correctly captures this, s.t., amplitudes and phases of the predicted sinusoidal functions are in accordance with the observed context data point.

(b) A second example on another instance of the sinusoidal function class, where the task posterior shows pronounced multimodality, which translates into a bimodal predictive distribution.

(c) Larger context sizes (three examples, red crosses) leave less task ambiguity, resulting in a unimodal and nearly isotropic task posterior distribution. Our GMM approximation again correctly approximates this distribution, making use of only two of the $K = 3$ mixture components (the mixture weight of the orange component is close to zero, so no samples from this component are observed).

Figure 12: Visualization of our GMM-NP model for a $d_z = 2$ dimensional latent space, trained on sinusoidal functions with varying amplitudes and phases, cf. Sec. 5.1. Left panels: unnormalized task posterior distribution (contours) and variational GMM approximation with $K = 3$ components (ellipses, mixture weights in $\%$). Right panels: corresponding samples from our model (blue lines), when having observed a context data set (red crosses), together with unobserved ground truth data (black dots). The visualizations show that (i) the true task posterior distribution can be highly correlated and multimodal, i.p., for small context sets (panels a,b), (ii) our variational task posterior approximation correctly approximates this distribution, which (iii) leads to expressive predictive distributions that incorporate both the inductive priors learned from the meta-dataset (all samples are sinusoidal in shape) and the additional information contained in the context set (all samples pass close to the context data).

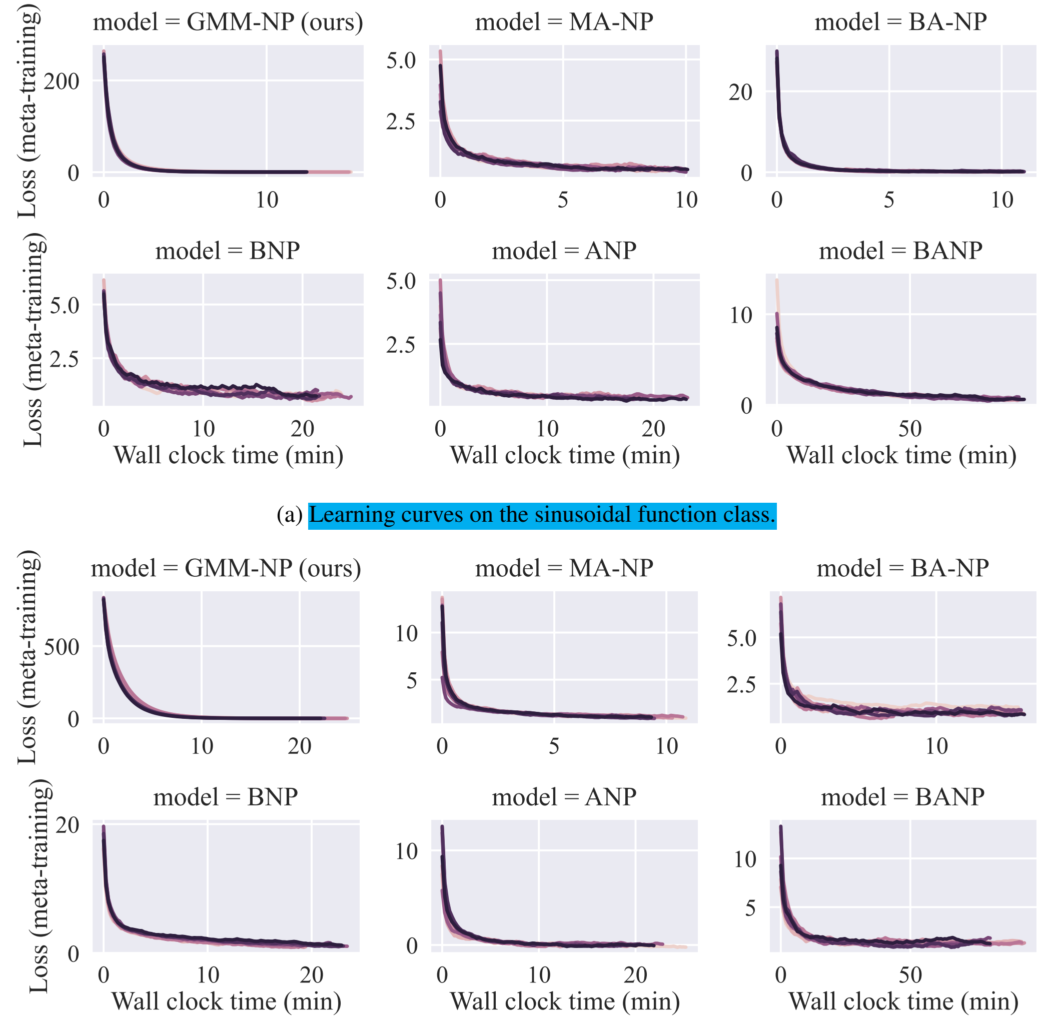

(a) Learning curves on the sinusoidal function class.

(b) Learning curves on the mix of affine and sinusoidal function class.

Figure 13: Learning curves for meta-training on the synthetic datasets, cf. Sec. 5.1. For each method, we show the learning curves for the 8 seeds used to compute the results presented in the main text. For GMM-NP, we show the loss for the decoder parameters $\boldsymbol{\theta}$, for the other methods we show the joint loss for the encoder and decoder parameters $(\boldsymbol{\phi}, \boldsymbol{\theta})$. Note that for GMM-NP, convergence of $\boldsymbol{\theta}$ implies convergence of the variational parameters $\boldsymbol{\phi}$. As discussed in Sec. 4, GMM-NP incurs a computational cost comparable to the baseline methods.

A.5.6 Runtime Comparison

We compare the runtime of our GMM-NP algorithm with the baseline methods on the synthetic tasks presented in Sec. 5.1.

Meta-Training. Fig. 13 shows the learning curves for meta-training corresponding to the results presented in the main part of this paper. As discussed in Sec. 4, GMM-NP incurs a computational cost comparable to the baseline methods.

Test-time Adaptation. As discussed in Sec. 4, GMM-NP does not amortize TP inference, i.e., it does not learn a set encoder architecture, but adapts new variational GMMs at test time. Naturally,

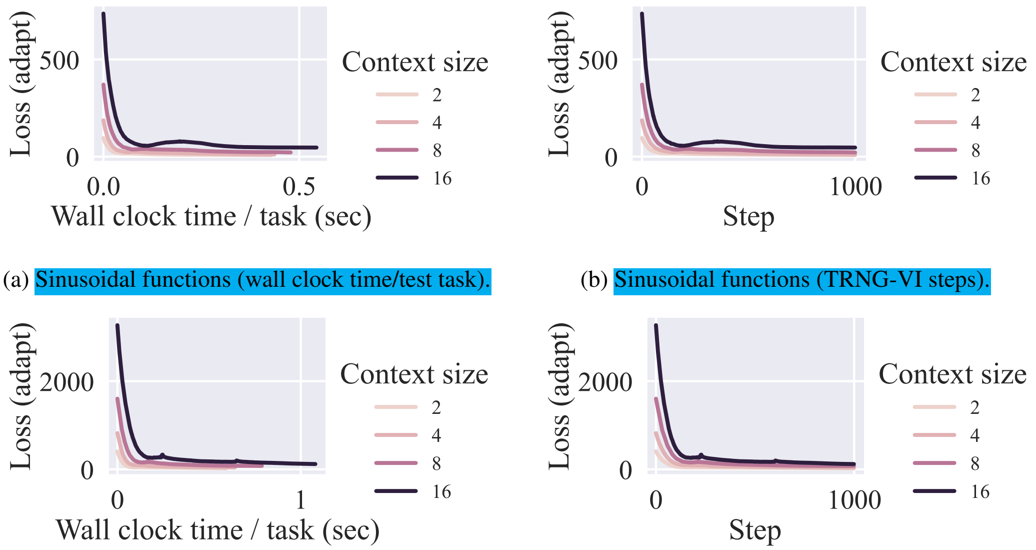

(a) Sinusoidal functions (wall clock time/test task).

(b) Sinusoidal functions (TRNG-VI steps).

(c) Mix of affine and sinusoidal functions (wall clock time/test task).

(d) Mix of affine and sinusoidal functions (TRNG-VI steps).

Figure 14: Learning curves for fitting variational GMMs to the test tasks by TRNG-VI (Arenz et al., 2022), as used by our GMM-NP (Sec. 4), on the synthetic datasets (Sec. 5.1). We show results for the range of context sizes used to compute the results in the main text. GMM-NP's TRNG-VI optimization converges in approx. 0.1 s – 1 s per test task (depending on the context set size).

this incurs a higher computational cost in comparison to amortized architectures, which compute predictions on test tasks in a single forward pass through their set-encoder – decoder architecture. In Fig. 14, we show the learning curves for fitting variational GMMs (by iterating Eqs. (8) to the test tasks and for the range of context sizes used to compute the results presented in Sec. 5.1. As stated in the main text, GMM-NP's TRNG-VI optimization converges in approx. 0.1 s – 1 s per test task (depending on the context set size).

Table 2: Results of our hyperparameter optimization on the sinusoidal function class. We provide the settings for the latent dimensionality d_z and the number of parameters of the BML models compared in Sec. 5.1. For models with deterministic paths, the encoder parameters also contain the parameters of attentive modules. For our GMM-NP, we also provide the number of GMM-components K. Furthermore, as GMM-NP does not amortize TP-inference but learns separate variational GMMs for each subtask generated from the meta-dataset (cf. Secs. 4 and A.3.2), we also provide the total number of variational GMM parameters during meta-training. Note that these variational GMMs are decoupled and can be optimized in parallel. Furthermore they are not required for predictions at test time and can be discarded after meta-training.

Model	d_z	K	No. of decoder parameters $\lvert\boldsymbol{\theta}\rvert$	No. of encoder/variational parameters $\lvert\boldsymbol{\phi}\rvert$ (per task)	No. of encoder/variational parameters $\lvert\boldsymbol{\phi}\rvert$ (meta-training)
GMM-NP (ours)	3	4	121	39	79872
MA-NP	10	-	2298	2595	2595
BA-NP	27	-	7334	7386	7386
BNP	56	-	12770	19488	19488
ANP	19	-	4096	10335	10335
BANP	40	-	6562	28320	28320

Table 3: Results of our hyperparameter optimization on the mix of affine and sinusoidal functions. We provide the settings for the latent dimensionality d_z and the number of parameters of the BML models compared in Sec. 5.1. For models with deterministic paths, the encoder parameters also contain the parameters of attentive modules. For our GMM-NP, we also provide the number of GMM-components K. Furthermore, as GMM-NP does not amortize TP-inference but learns separate variational GMMs for each subtask generated from the meta-dataset (cf. Secs. 4 and A.3.2), we also provide the total number of variational GMM parameters during meta-training. Note that these variational GMMs are decoupled and thus can be optimized in parallel. Furthermore, they are not required for predictions at test time and can be discarded after meta-training.

Model	d_z	K	No. of decoder parameters $\lvert\boldsymbol{\theta}\rvert$	No. of encoder/variational parameters $\lvert\boldsymbol{\phi}\rvert$ (per task)	No. of encoder/variational parameters $\lvert\boldsymbol{\phi}\rvert$ (meta-training)
GMM-NP (ours)	4	4	2289	59	120832
MA-NP	19	-	2562	3679	3679
BA-NP	30	-	11592	11650	11650
BNP	54	-	11882	18144	18144
ANP	30	-	4496	14448	14448
BANP	32	-	4226	18304	18304

A.5.7 Analysis of HPO results

As discussed in Secs. 5 and A.3, we optimized architectural hyperparameters individually for each model-dataset combination presented in our empirical evaluation, in order to arrive at a fair comparison of our GMM-NP with the baseline methods. In Tabs. 2 and 3, we provide the resulting settings for the latent dimensionality d_z, and the number of parameters of the BML models compared in Sec. 5.1. While the number of variational parameters during meta-training is naturally comparably high for non-amortizing methods such as GMM-NP, we observe that the expressive GMM-NP TP approximation allows comparably lightweight decoders and small latent dimensions. This is intuitive, as simple TP approximations require (i) large latent dimensions to encode relevant information in the latent space, together with (ii) expressive decoder architectures to transform the simple latent distribution into an expressive predictive distribution. Note further that the variational parameters belonging to different tasks are not coupled in non-amortizing architectures such as ours, which allows trivial parallelization of the variational optimization between tasks, explaining why the computational cost is easily managable, cf. Sec. A.5.6. Note also that the number of variational parameters one has to store and adapt for GMM-NP to make predictions on unseen test tasks is comparably small because the variational GMMs learned during meta-training can be discarded as they are not required for predictions at test time.